sustainability

MDPI

Article

Using Satellite-Based Evapotranspiration (ESTIMET) in SWAT to Quantify Sediment Yield in Scarce Data in a Desertified Watershed

Raul Gomes da Silva [1,*], Aline Maria Soares das Chagas [2], Monaliza Araújo de Santana [2], Cinthia Maria de Abreu Claudino [3], Victor Hugo Rabelo Coelho [3], Thayná Alice Brito Almeida [2], Abelardo Antônio de Assunção Montenegro [2], Yuri Jacques Agra Bezerra da Silva [2] and Carolyne Wanessa Lins de Andrade Farias [4]

[1] Department of Soil Science, Federal Rural University of Pernambuco, Recife 52171-900, PE, Brazil
[2] Department of Agricultural Engineering, Federal Rural University of Pernambuco, Recife 52171-900, PE, Brazil; monaliza.araujo@ufrpe.br (M.A.d.S.); thayna.britoalmeida@ufrpe.br (T.A.B.A.); abelardo.montenegro@ufrpe.br (A.A.d.A.M.)
[3] Department of Civil and Environmental Engineering, Federal University of Paraiba, Areia 58397-000, PB, Brazil
[4] Department of Geosciences, University of Paraiba, João Pessoa 58051-090, PB, Brazil
* Correspondence: raul.gomess@ufrpe.br

Abstract

The ESTIMET (Enhanced and Spatial-Temporal Improvement of MODIS EvapoTranspiration algorithm) model provides continuous, spatially distributed daily ET, essential for model calibration in data-scarce environments where conventional hydrological monitoring is unavailable. The challenge of applying SWAT in arid regions without ground observations, this study proposes a remote-sensing-based calibration approach using ESTIMET to overcome data scarcity. Daily satellite-derived evapotranspiration (ET) data to assess the performance of the Soil and Water Assessment Tool (SWAT) was used to evaluate the performance of the SWAT in a desertified watershed in Brazil, aiming to assess ESTIMET's effectiveness in supporting SWAT calibration, quantify sediment yield, and examine the influence of land-use changes on environmental quality over 21-years period. The results highlight a distinct hydrological response in SWAT initially underestimated ET, contrasting with patterns typically observed in other semi-arid applications and demonstrating that desertified environments require distinct calibration strategies. Performance indicators showed strong agreement between observed and simulated ET (R^2 = 0.94; NSE = 0.76), supporting satellite-based ET as a valuable source for improving SWAT performance in watersheds where empirical hydrometeorological data are sparse or unevenly distributed. Sediment yield was generally low to moderate, with degradation concentrated in bare-soil areas associated with deforestation.

Keywords: satellite-based evapotranspiration; ESTIMET model; Prediction in Ungauged basins; sediment yield; SWAT model

Check for updates

Academic Editors: George Nick Zaimes, Paschalis Koutalakis and Valasia Iakovoglou

Received: 17 November 2025
Revised: 2 January 2026
Accepted: 8 January 2026
Published: 16 January 2026

Copyright: © 2026 by the authors. Licensee MDPI, Basel, Switzerland. This article is an open access article distributed under the terms and conditions of the Creative Commons Attribution (CC BY) license.

1. Introduction

In semi-arid environments, the low percentage of vegetation cover leaves the soils exposed to wind and rain action, making these regions highly susceptible to erosion and sediment yield to the drainage network. These dynamics present challenges related to sustainability, because soil loss directly affects the viability of agriculture and ecosystem

health. According to the Sixth Assessment Report of the Intergovernmental Panel on Climate Change [1], abrupt climate changes and intensive human land use and land cover (LULC) increase the vulnerability of the Brazilian semi-arid zone to aridification, primarily due to more frequent and intense droughts. In this context, desertification is defined as the degradation of arid, semi-arid, and sub-humid lands, strongly associated with low precipitation and high evapotranspiration. Among the various forms of soil degradation, desertification poses one of the greatest threats to human livelihoods, requiring integrated approaches to sustainable development to mitigate its rapid impact on society compared to other degradation processes [2,3].

Within this context, the Cachoeirinha stream basin, within the Cabrobó Desertification Nucleus (CDN) in the Brazilian semi-arid region, stands out as an area of great importance for hydrosedimentological research due to its significant socio-economic and environmental implications [4]. The study in this basin can be characterized as Prediction in Ungauged basins (PUB) due to the development of studies in basins with insufficient measurement data, addressing the challenge of hydrological uncertainty through improved models, regional analysis, and new data techniques, crucial for water resource management and climate impact studies. These tools are vital for addressing the region's current environmental crisis, as it undergoes desertification, its socio-economic resilience may be compromised in both the short and long terms. Consequently, erosion assessment studies and the identification of areas susceptible to degradation become increasingly necessary to define and quantify sustainability limits within the territory. One way to evaluate environmental quality is by understanding the sediment yield (SY), which reflects the soil's susceptibility to erosion, as well as topographic conditions that favor such processes, a problem widely studied in Brazilian watersheds [5].

The SY can be defined as the amount of sediment per unit area removed from a watershed by flowing water during a specified period, serving as a measure of geomorphic activity and indicating changes in the desert ecosystem [6,7]. Furthermore, SY is important as it reflects sediment transfer at the catchment scale, highlights off-site impacts (reservoir sedimentation and flooding), and serves as a complementary desertification indicator. Therefore, SY data is essential to measure and monitor sustainability, providing insights into long-term responses to environmental changes [8].

To identify the areas within the basin most affected by SY from erosion, several models have been developed, particularly for applications at the watershed scale. Among available tools, the SWAT (Soil and Water Assessment Tool) is widely used to simulate hydrological processes, flow dynamics and sediment yield in both humid and dry regions [9–11]. According to previous studies [3,12], the model also seeks to predict the impacts of LULC and management practices on water resources, sediment generation, and nutrient loss at daily, monthly, or annual time steps. The broad applicability of the SWAT model comes from its ability to simulate processes at the watershed scale, serving as a robust sustainability tool applicable in a variety of environments [13].

The SWAT model was originally developed by the USDA Agricultural Research Service (ARS) after nearly 30 years of continuous experimentation with erosion models [14]. Specifically in semi-arid climates, the model is particularly valuable due to pronounced thermal amplitude and seasonal precipitation extremes, which generate sharp contrasts that influence sediment yield dynamics, and the observed data are limited, creating gaps in information that are difficult to fill, making research in this area unfeasible [15–17]. Under these conditions, SWAT enables the comparison of different SY models and helps capture system responses under both normal and extreme scenarios [13,14,18,19]. Currently, SWAT is one of the most widely used models in hydrological studies of river basins, particularly

for simulating LULC scenarios, thereby assisting watershed managers in decision-making and the formulation of policies relating to sustainability [20–22].

Traditionally, SWAT calibration relies on river flow monitoring, which requires continuous maintenance, while conventional evapotranspiration (ET) measurements are often limited in coverage and frequency, hindering model validation across heterogeneous landscapes [23]. To address these limitations, remote sensing offers a promising alternative through the Moderate Resolution Imaging Spectroradiometer (MODIS) and its MOD16 product. This dataset provides quasi-continuous, spatially distributed ET observations at a 500 m resolution across three temporal scales (8-day, monthly, and annual) [24]. Consequently, using the MOD16 product for SWAT calibration fills observational gaps and allows the model to better capture the temporal and spatial variability of water fluxes, improving the representation of hydrological processes [25].

The integration of remote sensing data further reduces uncertainties associated with sparse ground measurements, enabling robust assessments of basin-scale water balance and sediment transport [26]. While this synergy enhances model accuracy and supports management strategies in water-scarce regions [27,28], standard MOD16 products face limitations regarding resolution, cloud cover, and land use parameterization. To address these challenges, Claudino et al. [29] developed the ESTIMET model, which offers near-real-time, continuous daily ET at a 250 m resolution specifically for tropical biomes. By adjusting LULC parameters to Brazilian vegetation, refining stomatal conductance schemes, and minimizing data loss from cloud cover, ESTIMET better differentiates microclimates and vegetation types, resulting in more accurate ET estimations [29,30].

Despite advances in remote sensing and hydrological modeling, few studies have integrated high-resolution satellite-based ET products, such as ESTIMET, into SWAT calibration for sediment yield assessment in semi-arid regions undergoing desertification, particularly in tropical sandy soils. Building upon this advanced methodology, the main objective of this study is to conduct a spatial-temporal analysis of SY in the Cachoeirinha stream basin from 2000 to 2024 by integrating SWAT model with satellite-based ET data from ESTIMET. Specifically, this study aims to evaluate the potential of ESTIMET to support SWAT calibration, quantify sediment yield dynamics, and analyze the influence of land-use changes on environmental quality. By investigating these processes, it is possible to evaluate both the impacts of human activities and the effects of recent climate change on water resource quality in this region, providing a scientific basis for applications of sustainability and the development of effective environmental policies in data-scarce regions.

2. Materials and Methods

2.1. Study Area

The Cachoeirinha Stream watershed is located within the Cabrobó Desertification Nucleus (CDN), between the coordinates 08°16′94″–08°26′44″ S and 39°16′47″–39°05′39″ W. It forms part of the hydrological system of the middle São Francisco River basin as a sub-basin in the state of Pernambuco, within the morphoclimatic domain of the Caatinga. The watershed covers an area of 194 km^2, with its headwaters located in the southwestern portion of the municipality of Salgueiro-PE. The main channel extends for approximately 30 km before joining the Terra Nova Stream, a tributary of the São Francisco River, in the central region of the municipality of Cabrobó-PE (Figure 1).

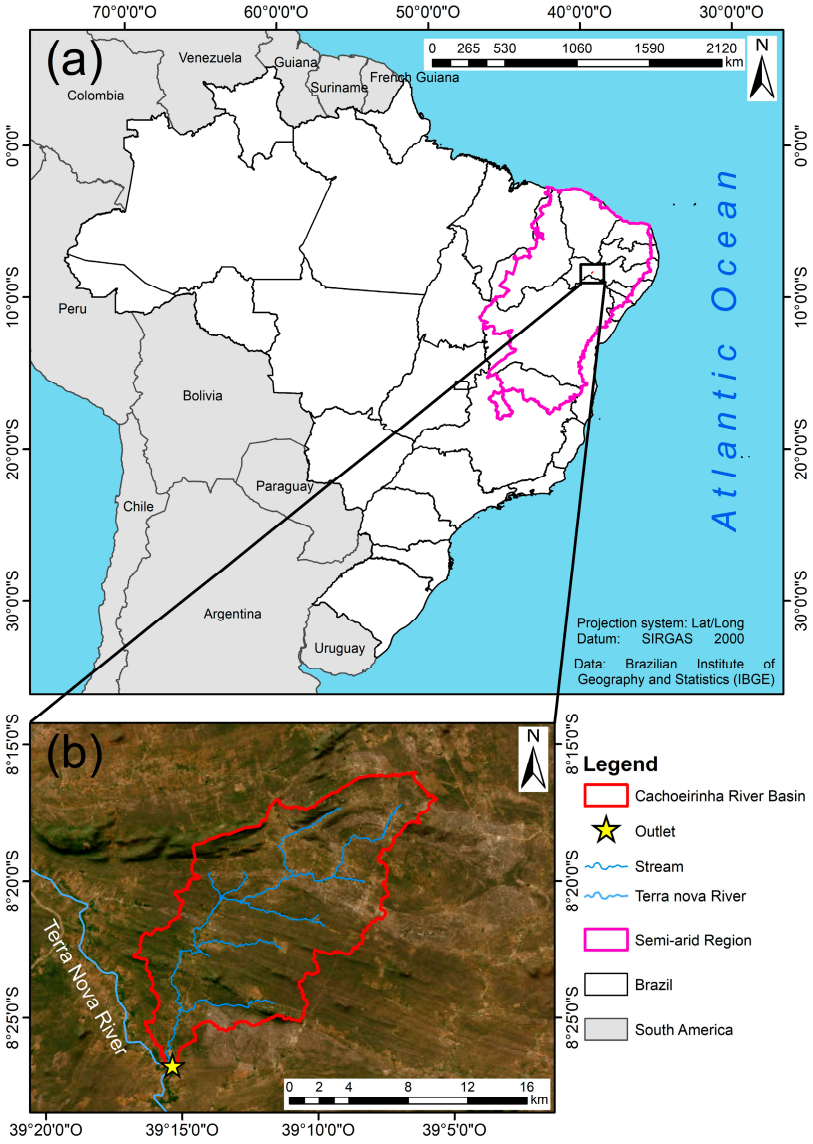

Figure 1. (**a**) Location of the Cachoeirinha River basin in semi-arid region, Pernambuco State (PE) of Brazil, (**b**) outlet and streamflow. Souce: Adapted from [30].

The climate of the region is classified by Köppen as semi-arid (BSh), characterized by low rainfall and highly irregular distribution [31]. According to records from Superintendence for the Development of the Northeast (SUDENE) (1961–1980) and National Institute of Meteorology (INMET) (1980–1990), for the period 1961–1990, the average annual rainfall in the CDN region was 541 mm [4]. More recent data from Pernambuco Water and Climate Association (APAC) [32] indicate a decline to 352 mm per year, representing a reduction of approximately 35%. This substantial decrease makes the region highly susceptible to soil degradation and desertification.

Figure 2 shows the climatic seasonality, with rainfall concentrated between January and April, reaching its peak in March (82.3 mm). From May onwards, there is a sharp decrease in precipitation, with almost no rainfall between July and September (less than 2 mm). Average temperature varies less throughout the year but still decreases during the dry period, with July recording the lowest value (16.9 °C), while the warmest months are January, February, and December, with values above 26 °C. This pattern characterizes a semi-arid climate, typical of the Brazilian Northeast hinterlands, with rainfall concentrated in a short-wet season followed by prolonged drought periods.

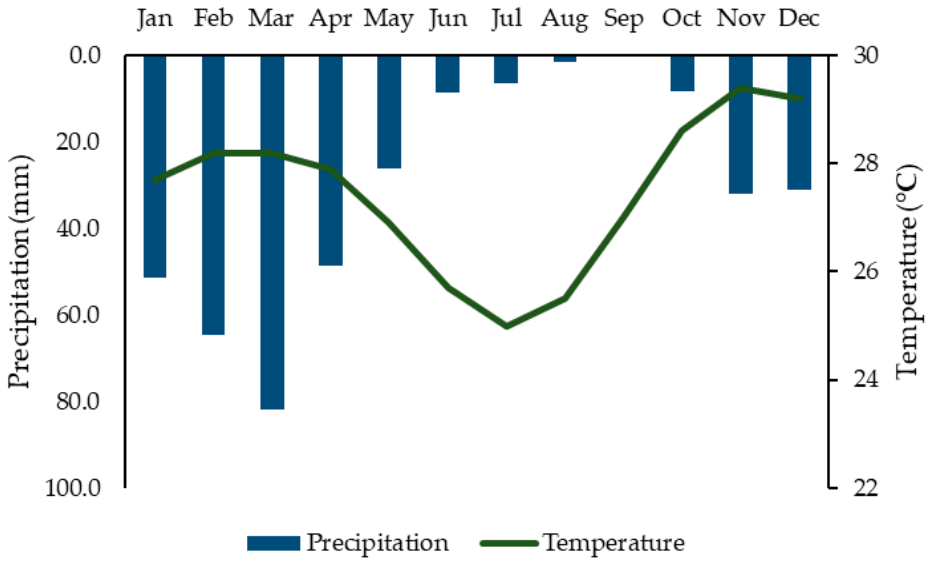

Figure 2. Monthly precipitation and temperature record (1994–2024).

The Caatinga biome, a seasonally dry tropical forest (SDTF) located in Northeastern Brazil, is characterized by shrubby and thorny vegetation adapted to prolonged droughts. The study area is predominantly covered by caatinga vegetation, especially shrubby caatinga (66%), characterized by spacing between plants that becomes more pronounced during the dry season. Agriculture and livestock occupy 32% of the area, directly affecting geoenvironmental conditions and surface sediment dynamics. The caatinga in the study area is dry deciduous, hyperxerophytic, and adapted to prolonged droughts [33]. Despite its relatively high susceptibility to erosion due to sparse vegetation cover and low leaf and root density, caatinga still provides greater protection against erosion compared to agricultural areas and bare soil [34]. This highlights the importance of preserving caatinga vegetation, not only for maintaining biodiversity but also for mitigating erosion and sediment yield.

In addition to its role in soil protection, the Caatinga also exhibits ecohydrological dynamics that strongly influence water balance processes. Transpiration, particularly in dryland forests, plays a major role in the water cycle, and the one-million-km^2 Caatinga biome is a data-scarce region in the Brazilian Semiarid, where rainy and dry seasons are clearly distinct. Dry regions have distinct ecohydrological processes, and this needs to be taken into account in hydrological modeling schemes. Because evapotranspiration patterns in semiarid environments are particularly complex, developing accurate hydrological balances requires model validation that explicitly considers evapotranspiration fluxes. Models calibrated with real evapotranspiration data help better represent these processes. Overall, such insights contribute to a better understanding of transpiration rates in dryland environments and may support water-resources management, since transpiration reflects local water use and availability [30].

2.2. Hydrosedimentological Simulation with SWAT

The SWAT (Soil and Water Assessment Tool) were developed by the USDA Agricultural Research Service, based on nearly 30 years of modeling experience [35]. The current version of SWAT performs continuous simulations of water resources in river basins on a daily time step. It is designed to predict and simulate the impacts of land and water man-

agement on hydrology and sediment transport across river networks, even at continental basin scales [9]. This daily simulation model can be expressed as follows Equation (1):

$$SW_t = SW_0 + \sum_{t=1}^{t} \left(R_{day} - Q_{surf} - ET - W_{seep} - R_f \right) \quad (1)$$

where SW_t is the final soil water content of day n (mm); SW_0 is the initial soil water content of day i (mm); t is the simulation period (days); R_{day} is the total precipitation of day i (mm); Q_{surf} is the surface runoff of day i (mm); ET is the evapotranspiration of day i (mm); W_{seep} is the water leaching through the soil profile of day i (mm), and R_f is the return flow of day i (mm) (all units in mm).

In SWAT, the soil erosion caused by rainfall and runoff is estimated using the Modified Universal Soil Loss Equation (MUSLE), first proposed by Williams [36]. MUSLE is an adaptation of the Universal Soil Loss Equation (USLE), developed by Wischmeier and Smith [37]. While the USLE predicts average annual soil loss as a function of rainfall kinetic energy, MUSLE replaces the rainfall erosivity factor with a runoff factor. This modification improves sediment yield estimation by eliminating the need to compute sediment delivery ratios from hillslopes to the channel network, which is particularly advantageous during extreme rainfall events.

The MUSLE proposed by Williams [36] is expressed as Equation (2):

$$sed = 11.8 \left(Q_{sur} \times q_{peak} \times area_{hru} \right)^{0.56} \times K_{USLE} \times C_{USLE} \times P_{USLE} \times LS_{USLE} \times CFRG \quad (2)$$

where sed is sediment yield (t), Q_{sur} is runoff volume (mm H_2O/ha), q_{peak} is the peak runoff rate (m^3/s), $area_{hru}$ is the HRU area (ha), K_{USLE} is the USLE soil erodibility factor (0.0013 t·m^2·h/(m^3·t·cm)), C_{USLE} is the USLE cover and management factor, P_{USLE} is the conservation practice factor, LS_{USLE} is the topographic factor, and $CFRG$ is the coarse fragment factor.

Surface runoff volume in SWAT is generally estimated by the Curve Number (CN) method developed by the Natural Resources Conservation Service (NRCS) (Equation (3)). According to Rallison and Miller [38], this method provides a consistent framework for estimating runoff under different LULC, soil, and hydrological conditions.

$$Q_{surf} = \frac{\left(R_{daily} - Ia \right)^2}{\left(R_{daily} - Ia + S \right)} \quad (3)$$

where $Qsurf$ is the accumulated runoff or excess precipitation (mm H_2O), Ia is the initial abstraction (including surface storage, interception, and infiltration prior to runoff, in mm H_2O), and S is the potential maximum retention (mm H_2O). The retention parameter S varies primarily with soil type, land use, management practices, slope, and antecedent soil moisture conditions (Equation (4)):

$$S = 25.4 \frac{1000}{CN} - 10 \quad (4)$$

where CN is the curve number for the given day. The initial abstraction Ia is commonly approximated as 0.2 S, which simplifies (Equations (3)–(5)):

$$Q_{surf} = \frac{\left(R_{daily} - 0.2S \right)^2}{\left(R_{daily} + 0.8S \right)} \quad (5)$$

2.3. Input Data

The data required for this study included a digital elevation model (DEM) with 10 m spatial resolution derived from the ASTER satellite, a LULC map with 30 m spatial resolution provided by the MapBiomas platform [39], and a soil type map from the Agroecological Zoning of Pernambuco [40]. Slope classes were defined based on the Technical Manual of Geomorphology [41], resulting in five categories for the study area: very flat (<3%), flat (3–8%), moderate (8–20%), steep (20–45%), and very steep (>45%) according to Figure 3.

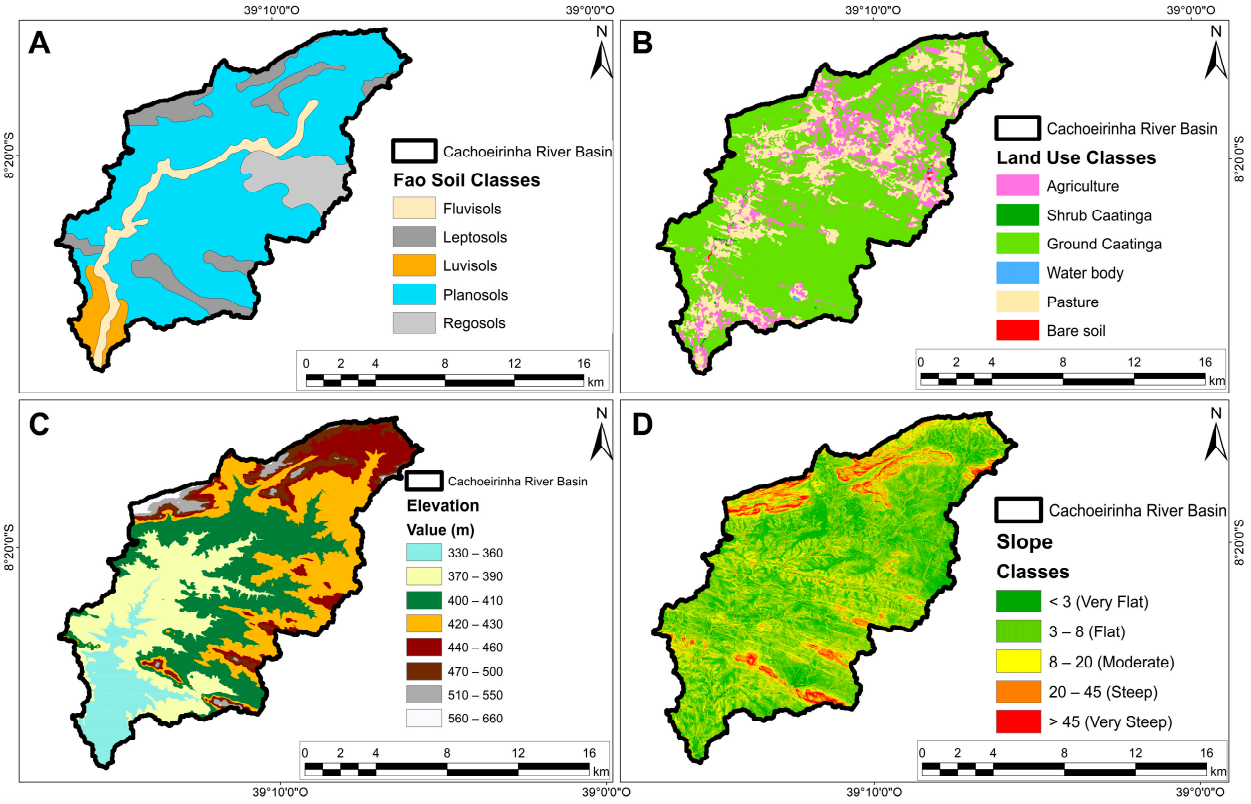

Figure 3. Maps of soil type (**A**), land use (**B**), elevation (**C**), and slope (**D**) of the Cachoeirinha watershed.

The combination of slope, soil, and land use information provides the basis for generating Hydrological Response Units (HRUs), which represent spatially homogeneous sub-environments that are essential for understanding erosion processes in river basins. In this study, 1578 HRUs and 99 sub-basins were delineated.

In addition to the maps, rainfall and meteorological data from two conventional rain stations, provided by the Pernambuco Water and Climate Agency (APAC), and two automatic weather stations, provided by the National Institute of Meteorology (INMET), were used (Table 1). These stations recorded all the meteorological variables required for hydrological simulations, including precipitation (mm), maximum and minimum air temperature (°C), relative humidity (%), wind speed ($m \cdot s^{-1}$), and solar radiation ($W \cdot m^{-2}$). The weather stations are located in the municipalities of Cabrobó and Salgueiro. To increase the robustness of the precipitation dataset, two conventional rain gauge stations, one in each municipality, were also incorporated (Figure 4).

Table 1. Climatological and rainfall stations used in the hydrological simulation.

Code	Name	Institute
A329	Cabrobó	INMET
82886	Cabrobó	APAC
A370	Salgueiro	INMET
D3870	Salgueiro	APAC

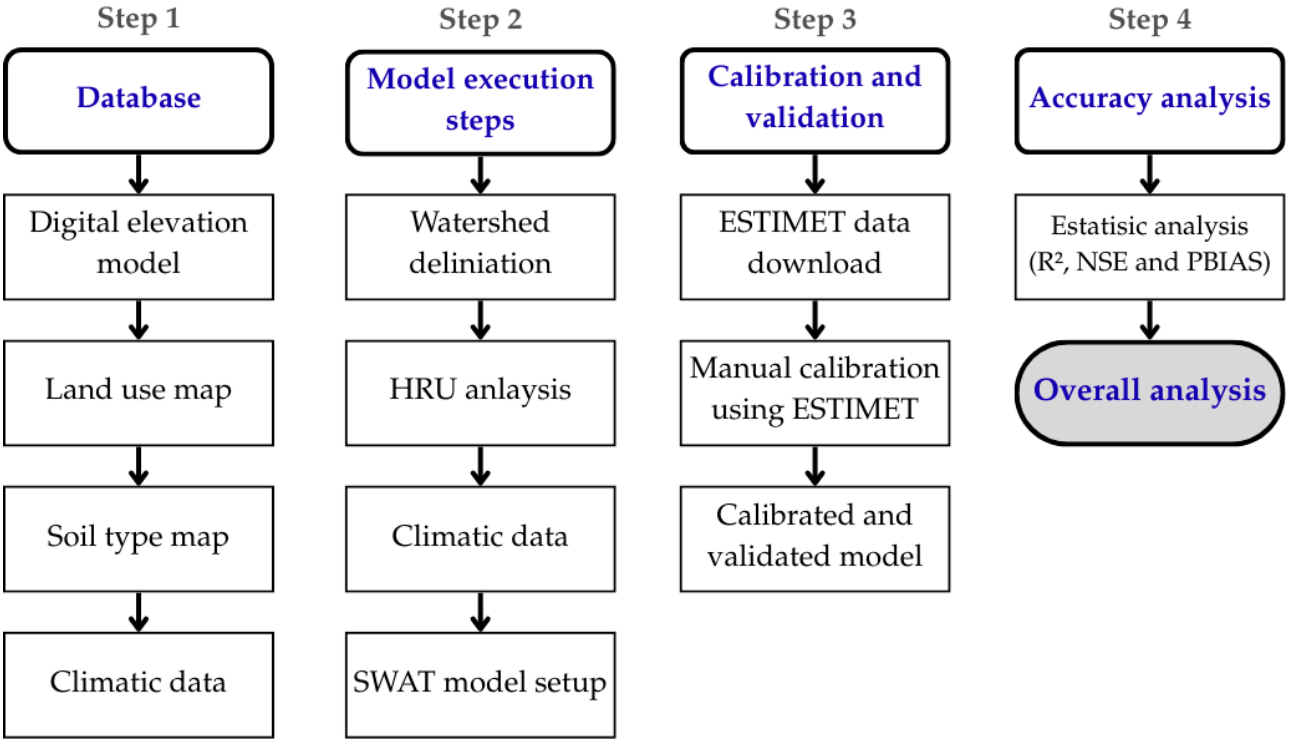

Figure 4. Flowchart including step-by-step research methodology, procedure for SWAT and ESTIMET.

2.4. Hydrological Simulation

The hydrological simulation was conducted using daily meteorological data from 2000 to 2024, with a 3-year warm-up period. Consequently, the outputs from 2003 to 2024 were considered and analyzed both as basin-wide averages and as monthly time series in a scale of sub-basin. The modeled results include actual evapotranspiration (ET), soil water content, precipitation, surface runoff, and Sediment Yield (SY). These variables were selected to better understand the climatic and hydrological dynamics of the basin, identify the main factors influencing water availability and quality in a desertified region, and evaluate erosion and sediment transport processes.

2.5. Evapotranspiration Data with ESTIMET

Previous studies [42–44] demonstrated that calibrating SWAT with satellite evapotranspiration (ET) is effective for ungauged basins in semi-arid with scarce or discontinuous streamflow data. Using the MOD16A2 product, they found ET better reflects the water balance in dry environments than runoff-based calibration, since rainfall largely converts to ET and river discharge is often intermittent.

Their work also showed that satellite ET improves the spatial representation of hydrological processes by integrating vegetation, land surface temperature, and energy balance dynamics, key factors in semi-arid climates.

This study adopts a similar approach but uses the ESTIMET algorithm instead of MOD16A2. ESTIMET offers higher spatial and temporal resolution and provides ET

estimates specifically adjusted for tropical dry forests, improving SWAT parameterization reliability under desertification conditions [23–25,27,45].

Similarly to MOD16, ESTIMET is based on the Penman-Monteith equation [26,43,46] to estimate the latent heat flux density (λE; W m^{-2}), which enables the derivation of total daily ET (mm) by applying a conversion factor. This total corresponds to the combined contributions of evaporation from the wet canopy surface (λE_{wet}), transpiration from vegetation under dry surface conditions (λE_{trans}), and evaporation from the soil (λE_{soil}) (Equation (6)).

$$\lambda E = \lambda E_{wet} + \lambda E_{trans} + \lambda E_{soil} = \frac{sA + \rho C_p (e_s - e_a)/r_a}{\Delta + \gamma\left(1 + \frac{r_s}{r_a}\right)} \quad (6)$$

where Δ represents the slope of the saturation vapor pressure–temperature curve (kPa °C^{-1}), A denotes the available energy (W m^{-2}), ρ is the air density (kg m^{-3}), C_p is the specific heat capacity of air at constant pressure (J kg^{-1} °C^{-1}), e_a refers to the actual water vapor pressure (kPa), e_s to the saturated vapor pressure (kPa), r_s is the surface resistance (s m^{-1}), r_a is the aerodynamic resistance (s m^{-1}), and γ is the psychrometric constant (kPa °C^{-1}). The validation of ESTIMET by Claudino et al. [29] indicated that in Brazil, the model captured the daily seasonal variations in ET observed by eddy covariance data, especially in the Caatinga biome, exhibiting better performance than that of global satellite-based products (e.g., MOD16A2GF, GLEAM 4.1a, and PML_V2).

2.6. Calibration, Validation, and Statistical Indicators of Model Evaluation

Eight years of monthly ESTIMET data (2003–2010) were used for manual calibration [43] in the QSWAT environment. Although the automated calibration techniques are less time-consuming, the parameters obtained through the automatic calibration process are often unrealistic [47]. In contrast, manual calibration relies on the modeler's experience and knowledge of the data properties and characteristics of the watershed system [48].

Before manual calibration, an analysis using SWAT-CUP was conducted to identify the most sensitive parameters. From the SWAT-CUP results, the parameter set with the highest SUFI-2 rating was selected for calibration with the SWAT Calibration Helper. Therefore, calibration focused on three parameters (Table 2): SOL_K (saturated hydraulic conductivity factor), SOL_AWC (available water capacity factor), and ESCO (soil evaporation compensation factor).

Table 2. Parameters used in calibration.

No.	Parameter	Calibrated Value
1	r_sol_k	0.2
2	r_sol_awc	2.5
3	r_esco	0.05

For calibration, two drought-period subsets were selected (Figure 5): August 2005 to January 2006 (Period A) and May 2006 to December 2006 (Period B), both in the dry season. The validation period extended from October 2009 to July 2010. The performing datasets were then organized into three groups, with Groups A and B used for calibration and an additional group reserved for validation.

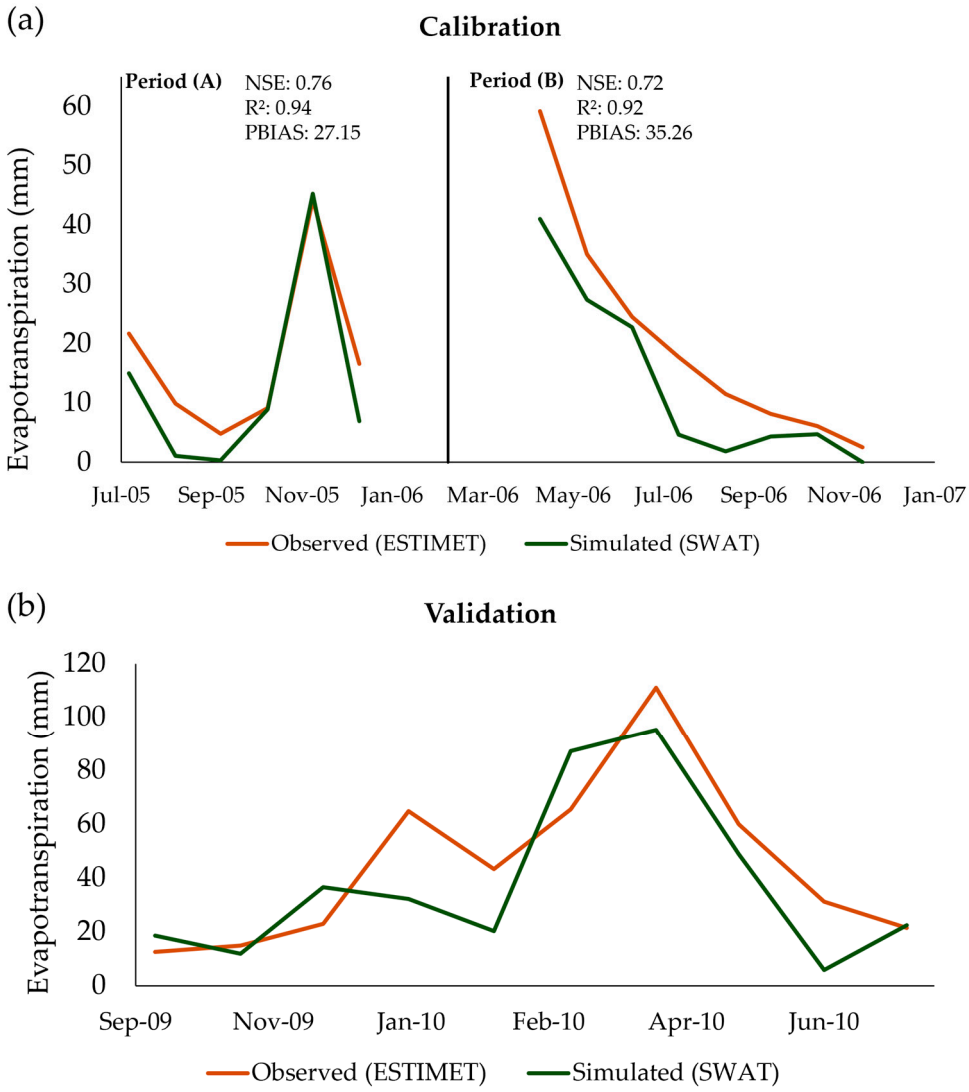

Figure 5. Statistical results of the calibration (**a**) and validation (**b**) of SWAT-simulated and ESTIMET model for evapotranspiration.

Calibration and validation performance of SWAT in simulating in actual evapotranspiration, were evaluated through statistical analysis based on the coefficient of determination (R^2), which describes the degree of collinearity between simulated and measured data, the Nash-Sutcliffe coefficient (NSE), a normalized statistic that assesses the relative magnitude of the residual variance ("noise") compared to the measured data variance ("information") where is the best objective function to reflect the overall fit of a hydrograph, and the percent bias (PBIAS) [46] an indicator that evaluates the average tendency of the simulated data to be larger or smaller than their observed counterparts and it is frequently used to measure water balance errors and has the capability to reveal poor model performance (Equations (7)–(9)). These performance evaluation criteria were recommended by Moriasi et al. [49] for hydrological models, considering the calibrated variable, and the time scale used in the calibration and validation processes.

$$R^2 = \frac{\left[\sum_{i=1}^{n}\left(Q_{obs}(i) - \overline{Q_{obs}}\right)\left(Q_{sim}(i) - \overline{Q_{sim}}\right)\right]^2}{\sum_{i=1}^{n}\left(Q_{obs}(i) - \overline{Q_{obs}}\right)^2 \sum_{i=1}^{n}\left(Q_{sim}(i) - \overline{Q_{sim}}\right)^2} \quad (7)$$

$$NSE = 1 - \left[\frac{\sum_{i=1}^{n}\left(Q_{obs}(i) - Q_{sim}\right)^2}{\sum_{i=1}^{n}\left(Q_{obs}(i) - Q_{obs}\right)^2}\right] \quad (8)$$

$$PBIAS = \left[\frac{\sum_{i=1}^{n}(Q_{obs}(i) - Q_{sim}(i)) \times 100}{\sum_{i=1}^{n} Q_{obs}(i)}\right] \quad (9)$$

where Q_{obs} represents the observed actual evapotranspiration from ESTIMET, Q_{sim} the simulated actual evapotranspiration on day i, and Q_{obs} and Q_{sim} denote the mean observed and simulated actual evapotranspiration, respectively. The coefficient of determination (R^2) ranges from 0 to 1, with 0 indicating no correlation and 1 representing perfect agreement with minimal error variance. The Nash–Sutcliffe Efficiency (NSE) can take values from $-\infty$ to 1; values less than or equal to 0 suggest poor model performance, while values approaching 1 indicate a close match between simulated and observed data. PBIAS measures the average tendency of the simulated values to be over- or underestimated, with an ideal value of 0. Positive PBIAS indicates underestimation, whereas negative values indicate overestimation. For monthly simulations at the watershed scale, the model's performance is generally considered satisfactory when R^2 exceeds 0.60, NSE is greater than 0.50, and PBIAS falls within ±25% [29,49,50].

3. Results

3.1. Calibration and Performance of SWAT Model

The calibration phase of the SWAT model achieved high performance, with R^2 values of 0.94 and 0.92 for Periods A and B, respectively, as show in Figure 5a. NSE values were also good, at 0.76 for Period A and 0.72 for Period B. However, PBIAS indicated moderate performance in Period A (27.15%) and Period B (35.26) reflecting a slight underestimation of ET. During validation, the model presented the best PBIAS performance, with PBIAS = 15.29%, but with moderate R^2 and NSE (R^2 = 0.69 and NSE = 0.61).

The dry periods exhibited better performance and greater agreement between observed and simulated data. These periods enabled improved model adjustment, showing that SWAT was more accurate in reproducing the dynamics of low water availability.

3.2. Annual Dynamics of Hydrosedimentological Processes

The statistical results of the simulated variables are presented in Table 3. The average annual precipitation was 449.2 mm, with a high interannual variability (SD = 171.2 mm), reflected in the wide range between maximum and minimum values. This irregular rainfall regime is the main driver of other hydrological processes. Surface runoff was low (average 22.8 mm), representing only about 5% of total precipitation. This low runoff-to-precipitation ratio suggests high soil infiltration capacity under predominantly gentle slope conditions. However, the standard deviation of runoff exceeded the mean, highlighting the basin's susceptibility to rapid and intense flows during concentrated torrential rainfall events.

Table 3. Descriptive statistics of hydrosedimentological variables.

	Precipitation (mm)	Surface Runoff (mm)	Soil Water (mm)	Evapotranspiration (mm)	Sediment Yield (ton/ha)
Maximum	900.58	100.35	228.2	518.83	7.45
Minimum	184.75	1.22	40.35	137.78	0.04
Mean	449.2	22.81	115.71	254.95	1.10
Standard Deviation	171.23	24.59	45.10	95.66	1.59

Soil water storage mean was 115.7 mm, and remained relatively stable over the period, acting as a key reservoir sustaining vegetation between rainfall events. This storage was replenished by infiltration and depleted mainly by ET, the largest water balance flux (254.95 mm on average), which accounted for approximately 63% of total precipitation. ET

thus emerged as the primary water loss pathway, consistent with the high atmospheric demand of ungauged basins in semi-arid environments.

Annual SY was relatively low (1.1 t ha^{-1} yr^{-1}), indicating general geomorphological stability under normal conditions. Nevertheless, its highly skewed distribution (maximum 7.5 t ha^{-1} yr^{-1}; SD = 1.6) revealed a strong association between soil erosion and extreme rainfall-runoff events. Overall, the basin's hydrological and erosive dynamics are dominated by localized, intense climatic events that generate disproportionate peaks of runoff and soil loss, superimposed on a background of low water availability and relative stability.

3.3. Correlation Coefficient Between Modeling Variables

Surface runoff proved to be the critical factor influencing SY, as demonstrated by the strong correlation between the two variables (R^2 = 0.84) and the coinciding peaks and troughs (Figure 6a). In contrast, soil water storage exhibited a weak relationship with SY, with no clear pattern detected (R^2 = 0.05; Figure 6b). Precipitation also showed limited correlation with SY (R^2 = 0.24; Figure 6c). Surface runoff itself was only moderately correlated with precipitation (R^2 = 0.49; Figure 6d), indicating that not every rainfall event generates runoff. In most cases, even intense rainfall fails to exceed the soil's storage capacity, so infiltration dominates over surface runoff.

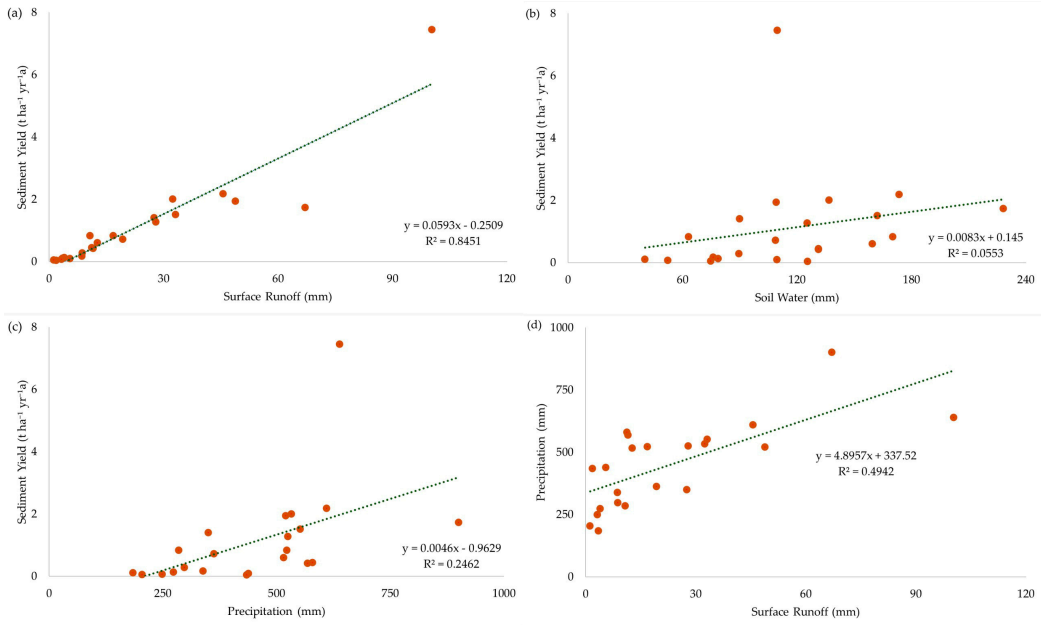

Figure 6. Coefficient of determination (R^2) between annual mean values of sediment yield and surface runoff (**a**), sediment yield and soil water (**b**), sediment yield and precipitation (**c**) and precipitation and surface runoff (**d**) in Cachoeirinha Basin.

A strong correlation was observed between precipitation and soil water (R^2 = 0.80; Figure 7a), as well as between precipitation and ET (R^2 = 0.73; Figure 7b), highlighting the dependence of both processes on rainfall input. A similarly high correlation was found between soil water and ET (R^2 = 0.79; Figure 7c).

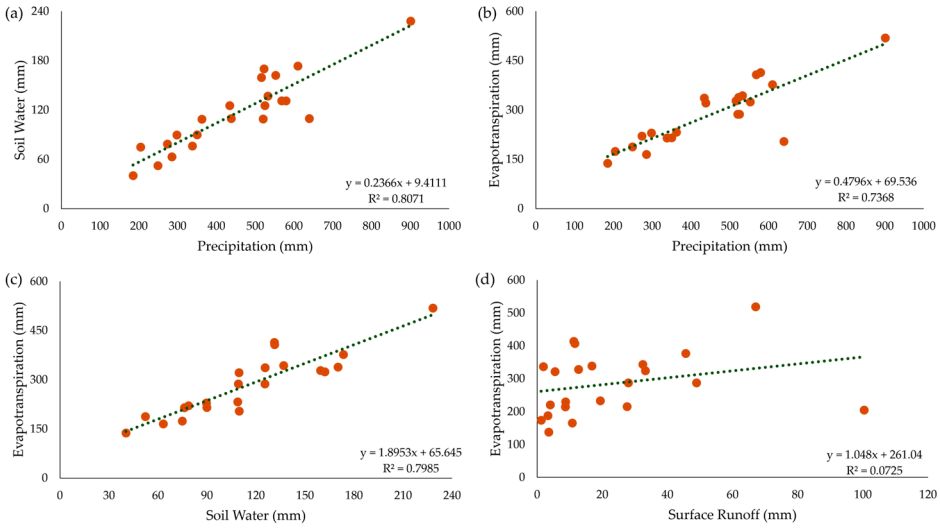

Figure 7. Coefficient of determination (R^2) between annual mean values of Soil water and precipitation (**a**), evapotranspiration and precipitation (**b**), evapotranspiration and soil water (**c**) and evapotranspiration and surface runoff (**d**) in Cachoeirinha Basin.

The annual temporal analysis (Figure 8) reveals a severe drought between 2012 and 2017, with 2012 standing out as the most critical year (184.75 mm of precipitation). During this period, all SWAT-simulated variables showed marked reductions. In 2012, surface runoff reached only 3.5 mm, while SY dropped to 0.11 t ha^{-1} yr^{-1}, the lowest value in the time series.

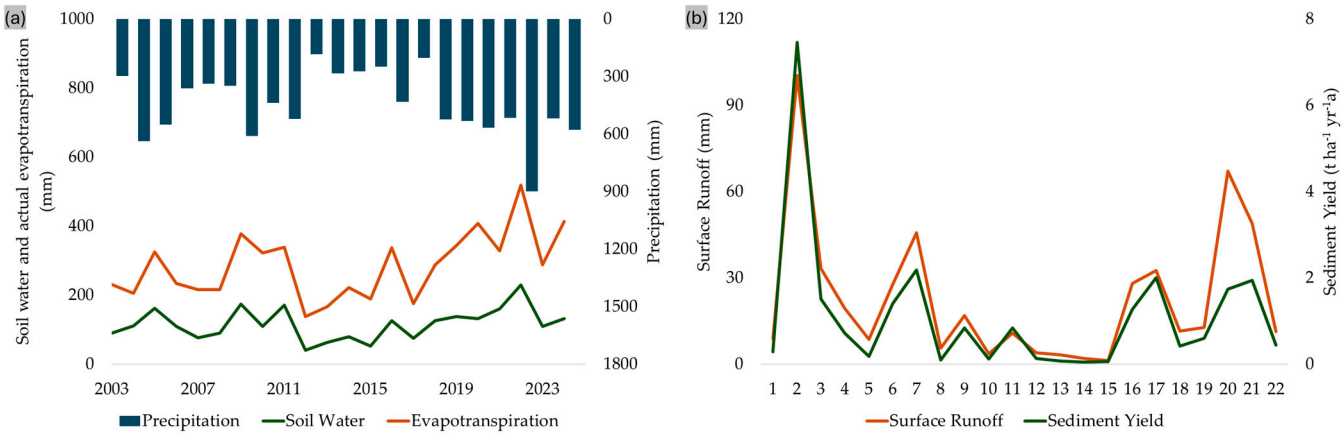

Figure 8. Annual time series of simulated soil water and actual evapotranspiration (**a**) and surface runoff and sediment yield (**b**) in the Cachoeirinha Basin from 2003 to 2023.

In contrast, the most recent years showed an increase in precipitation and related variables, peaking in 2022. That year was characterized by intense rainfall across northeastern Brazil, and SY values of 1.73 t ha^{-1} yr^{-1} in 2022 and 1.94 t ha^{-1} yr^{-1} in 2023 was observed. Soil water storage also peaked during this wetter period, reaching 228.2 mm in 2022 and 109.09 mm in 2023.

3.4. Spatial Variability of Hydrosedimentological Processes

High SY values (2.09–6.35 t ha^{-1} yr^{-1}) were strongly associated with Regosols, as shown by the red patches in Figure 9A. Other areas of moderate SY were linked to elevated surface runoff, particularly near the drainage network, represented by red and orange tones in Figure 9B. Soil water distribution (Figure 9C) was concentrated close to the drainage channel and near the basin outlet, overlapping with Luvisol patches. Conversely, soil water

was lower in higher-altitude and steeper areas, corresponding mainly to Regosols and sandy Leptosols.

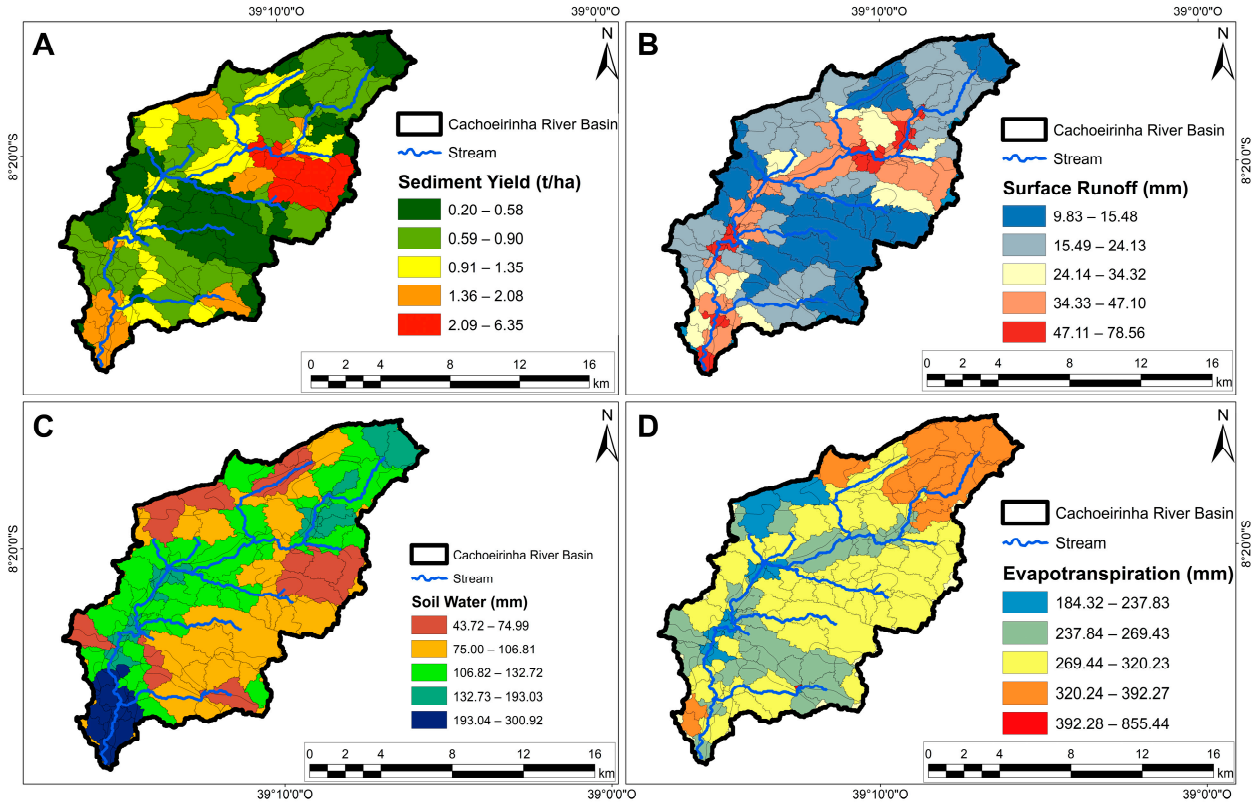

Figure 9. Sediment yield (t ha^{-1} yr^{-1}a) (**A**), surface runoff (mm) (**B**), soil water (mm) (**C**), and evapotranspiration (mm) (**D**) of the Cachoeirinha watershed.

Visually, the red zones of high SY also exhibited low soil water content, reinforcing that Regosols are not only more erosion-prone but also have reduced water retention capacity. Areas with higher ET (Figure 9D) were located near the drainage channel, where water availability is naturally greater, elevation is lower, and proximity to the water table is higher. ET was also more pronounced in the northeastern portion of the watershed, close to the headwaters, with an additional hotspot near the outlet due to increased water availability.

3.5. Monthly Dynamics of Climate and Hydrosedimentological Processes

The period of highest rainfall in the study area is between January and April, which coincides with higher ET rates and available soil water, as shown in Figure 10a. Collischonn and Tucci [46] observed that increased rainfall is generally associated with decreased evapotranspiration. However, in this study and in the studies by Lins et al. [50], it was observed that this result is more associated with the role of soil moisture in actual evapotranspiration, especially in regions of Tropical Seasonally Dry Forests (FTSS), where the variable that contributes most to ET is soil moisture (SW).

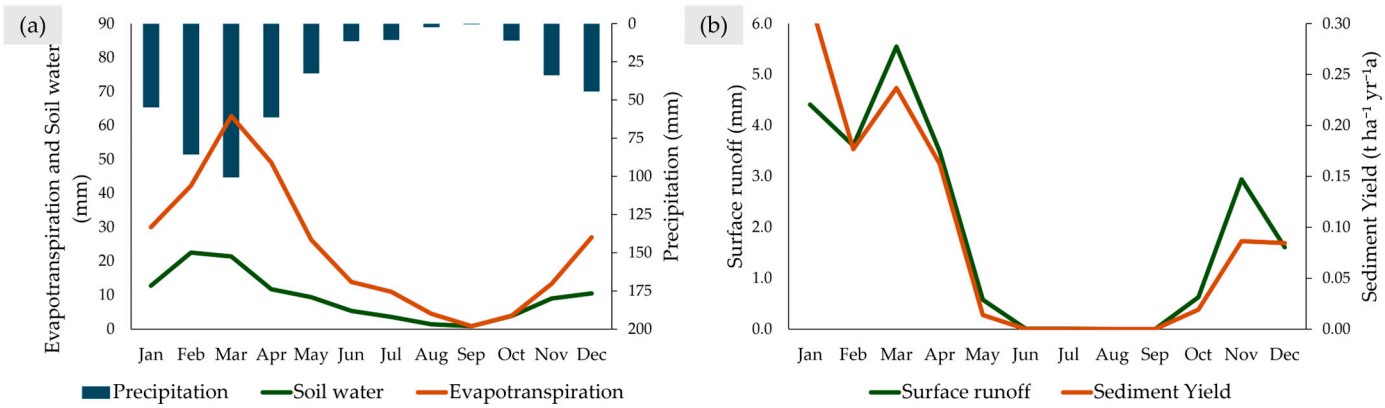

Figure 10. (**a**) Monthly distribution of evapotranspiration, soil water, and precipitation (mm); (**b**) Monthly distribution of surface runoff (mm) and sediment yield (t ha^{-1} yr^{-1}a). Monthly variation in precipitation, evapotranspiration, surface runoff, soil water, and sediment yield simulated by the SWAT model.

When evaluating the behavior of surface runoff and SY during the year (Figure 10b), it is observed that the increase in surface runoff volume is accompanied by an increase in the volume of sediments transported, indicating a direct relationship between them. However, the highest SY occurs during January, which is a transition month between the dry and rainy seasons, and not in March, which is the rainiest month. This can be explained by the fact that, during the transition period, rainfall events affect vegetation with low leaf cover due to the dry season, due to a characteristic of Caatinga vegetation, and therefore have greater erosive potential than rainfall during the rainy season, when vegetation has already recovered.

According to Daramola et al. [51] there is a strong and direct relationship between precipitation, surface runoff, and SY, with precipitation playing the main and most influential role. During rainy days, water flows over the Earth's surface, exposing fragile soil and rocks to erosion processes, and resulting in a sediment load.

3.6. Influence of Soil Types on Hydrological Processes

Figure 11 presents the boxplot of hydrological variables by soil type. Surface runoff showed partially heterogeneous behavior among the soil classes, generally ranging between 20.74 mm and 36.33 mm, with no major contrasts for most soils. The main exception was Leptosols, which recorded the lowest runoff (20.74 mm).

Because SY is strongly dependent on surface runoff, Leptosols also exhibited the lowest average SY (0.81 t ha^{-1} yr^{-1}). This result is explained by their landscape position, typically in flatter areas and closer to the main channel, which limits concentrated runoff and consequently reduces sediment transport.

Regosols, in contrast, showed the highest annual SY (2.47 t ha^{-1} yr^{-1}), associated with relatively high runoff (31.04 mm). This pattern is linked to their topographic setting, particularly in upper slopes and steep hillslopes, where shallow effective depth and low water retention (96.75 mm) enhance erosion. Their sandy texture and low organic carbon content further increase soil vulnerability. In the study area, this condition is intensified by predominantly agricultural land use, which amplifies soil exposure and accelerates erosion.

Regarding Fluvisols, this soil type exhibited higher soil water content (143.71 mm) due to their proximity to the fluvial channel. Luvisols also showed greater storage capacity (214.48 mm). Nevertheless, the highest ET was observed in Leptosols (298.11 mm), while Regosols presented the lowest ET (264.98 mm), consistent with their reduced water storage capacity.

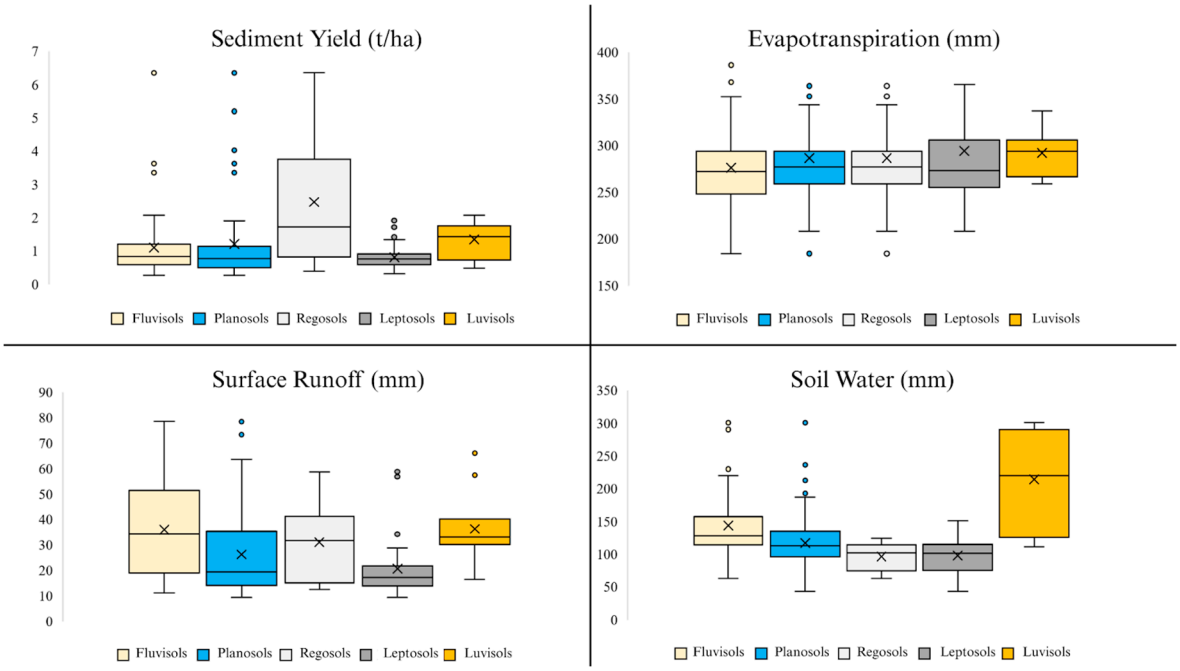

Figure 11. Boxplots of the simulated variables by soil type for the annual average series in the period between 2003 and 2024 for each sub-basin simulated by the SWAT model.

3.7. Influence of Land Use and Land Cover on Hydrological and Sediment Dynamics

Figure 12 shows the contribution of different LULC to SY, ET, surface runoff, and soil water. ET exhibited low variation among LULC, with the highest average in pasture (289.32 mm) and the lowest in arboreal caatinga (262.90 mm). Surface runoff was greatest in bare soil and shrub caatinga, with values of 33 mm and 32.82 mm, respectively, whereas the lowest runoff occurred in sparse caatinga (27.15 mm). Although annual soil water content varied minimally across LULC, shrub caatinga presented the highest average (143.68 mm), while exposed soil had the lowest (113.78 mm).

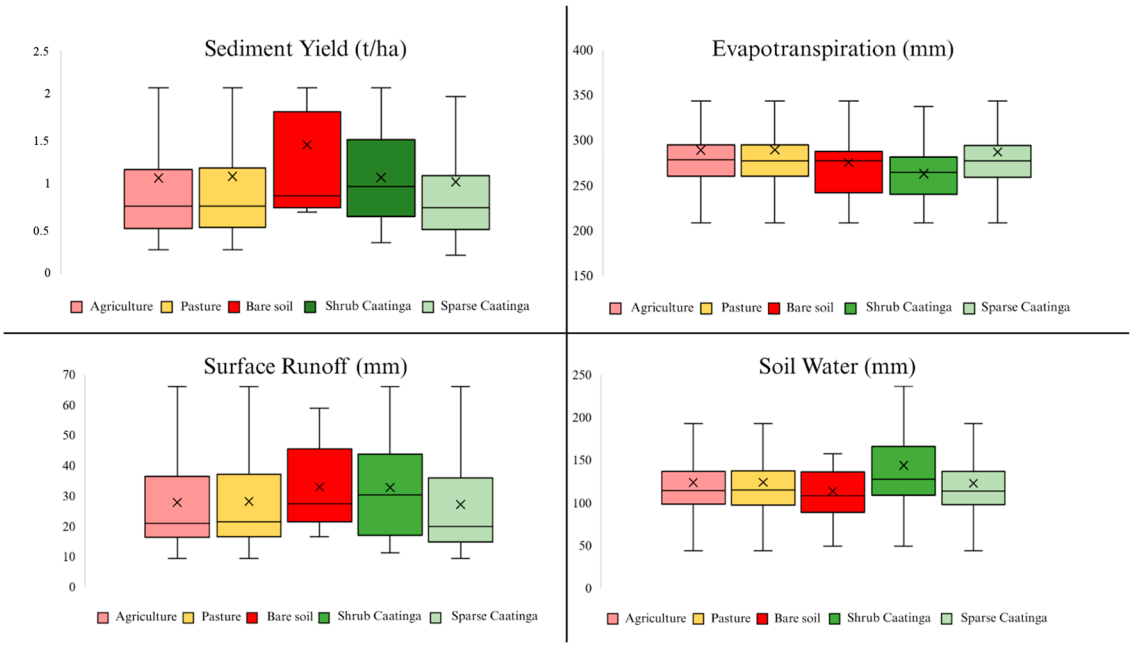

Figure 12. Boxplox of variables by LULC for the annual average series in the period between 2003 and 2024 for each sub-basin simulated by the SWAT model.

Regarding SY, an inverse pattern is observed compared to soil water content, exposed soils exhibit higher SY values (approximately 1 t ha^{-1}) than sparse and shrubby caatinga, which recorded initial soil loss around 0.4 t ha^{-1}. Furthermore, sediment yield varies more widely among other LULC classes, reaching up to 2.2 t ha^{-1}, whereas uncovered soils show a narrower range, from 1 to 2.2 t ha^{-1} (Figure 13).

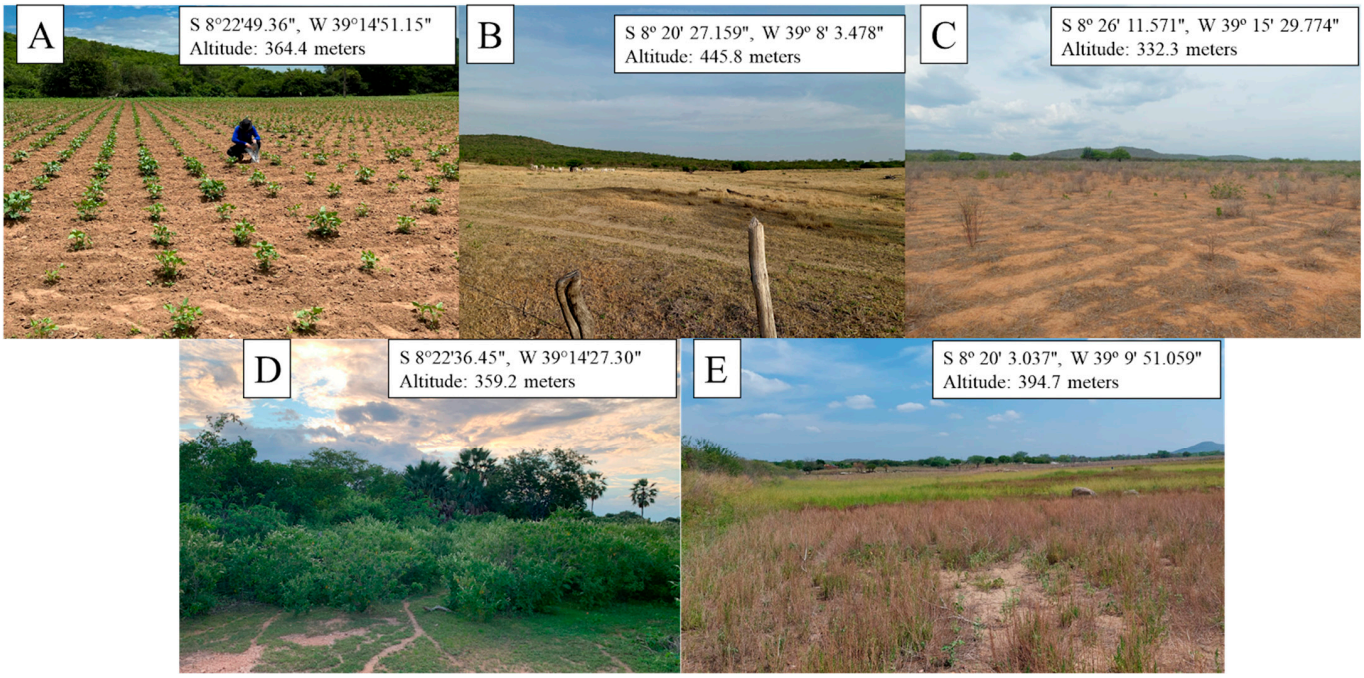

Figure 13. LULC classes: agriculture (**A**), pasture (**B**), bare soil (**C**), shrub caatinga (**D**), sparse caatinga (**E**) in the Cachoeirinha watershed. Source: The author.

4. Discussion

4.1. Calibration and Validation

Parameterization was a crucial step in this study. Since simulated evapotranspiration was lower than observed, an approach opposite to that commonly adopted in studies using satellite-based ET, or your set of parameters did not perform well for this study, making it difficult to find an optimal combination of parameters [25,45,50,51].

The parameters used were SOL_AWC, SOL_K, and ESCO. SOL_AWC was increased to enhance soil water capacity, while hydraulic conductivity (SOL_K) was reduced to limit lateral flow and rapid infiltration, thereby favoring evapotranspiration.

High R^2 and good NSE values in both calibration periods indicate that SWAT adequately reproduced the temporal dynamics of ET, confirming its ability to capture variability under semi-arid conditions. Nevertheless, PBIAS revealed a systematic underestimation, particularly in calibration Period B, likely due to the model's limitations in representing processes during prolonged droughts, when soil moisture is extremely low. In contrast, during Validation, the bias decreased, suggesting greater model consistency under intermediate or recovery moisture conditions. These results indicate that SWAT is robust in capturing seasonal ET patterns, although it tends to underestimate absolute values, a limitation also reported in other semi-arid applications [46].

According to Montenegro and Ragab [52], the selection of specific calibration and validation periods in arid and semi-arid environments is necessary to account for climate variability and the fragmentation of hydrological processes, thereby enhancing the reliability of simulations.

Seasonal behavior was more pronounced in years with higher water availability, when observed ET peaks were not fully captured by the model. Conversely, during months of low ET, SWAT often approached near-zero values, while observed data still indicated non-negligible magnitudes, contributing to the positive bias. Despite overall satisfactory performance, SWAT tended to underestimate ET peaks compared to MODIS, smoothing seasonal variability, a tendency also reported in other studies.

For instance, Lins et al. [50] found that 74% of precipitation was converted into ET (534.7 mm), reporting NSE values of 0.80 and 0.75 for calibration and validation, respectively, with PBIAS ranging from 16.7% to 17.2%. Similarly, Lins et al. [44] observed adequate performance (NSE = 0.67 for calibration and 0.74 for validation) but emphasized that SWAT tends to underestimate water retention during dry months. In contrast, the present study showed better performance under dry conditions, achieving R^2 = 0.98 for this period.

Other studies have reported comparable results, with variations depending on climatic and physiographic conditions. Silva et al. [53] highlighted the occurrence of intense, sporadic rainfall events in semi-arid basins, which can generate flow peaks even during dry periods, complicating calibration. Rocha et al. [54] reported strong agreement between SWAT-simulated ET and MODIS data, with NSE = 0.80 and R^2 = 0.86, confirming the model's ability to reproduce seasonal dynamics.

Zhang et al. [55], using parameter regionalization, obtained satisfactory performance (R^2 = 0.81, NSE = 0.75, PBIAS = –11.7%), while Parajuli et al. [27] reported values up to R^2 = 0.82 in calibration and 0.78 in validation. Franco and Bonumá [56] achieved R^2 = 0.51 in calibration and 0.80 in validation, although PBIAS values between 33% and 41% were considered unsatisfactory. Koltsida and Kallioras [28] also observed good consistency (R^2 = 0.86, NSE = 0.70, PBIAS = 6.1%), despite slight underestimation of simulated ET.

4.2. Correlation Coefficient Between Hydrological Variables

Surface runoff was identified as the primary driver of SY in the basin, highlighting the strong dependency of erosive processes on the hydrological response. Similar patterns have been reported in semi-arid basins, where rainfall concentrated in short, intense events promotes rapid runoff generation and sediment detachment [55,56].

In contrast, soil water storage showed no significant relationship with SY, and precipitation was only weakly correlated. This suggests that rainfall alone is insufficient to trigger erosion; rather, runoff generation is the determining factor. A similar behavior was reported by Montenegro and Ragab [52], who noted that infiltration often predominates in semi-arid soils, limiting runoff even during heavy rainfall events.

Correlation analysis also confirmed the dependency of soil water and ET on rainfall inputs, as well as a strong association between soil water and ET. The moderate relationship between precipitation and surface runoff indicates that not all rainfall events effectively generate runoff, since infiltration often exceeds the soil's saturation threshold. This result reinforces the understanding that semi-arid basins are highly sensitive to rainfall distribution rather than total rainfall volume [57].

4.3. Rainfall Seasonality in Semi-Arid Regions

The results reveal a clear seasonal pattern in the watershed's hydrosedimentological dynamics. Precipitation is concentrated between January and April, with March being the wettest month. This seasonal rainfall regime directly affects surface runoff and SY, which peaked in March. Similar patterns have been observed in semi-arid basins worldwide, where short, intense rainy periods concentrate most of the annual runoff and sediment transport [58–60].

During the dry season (May–September), rainfall is minimal, and both surface runoff and sediment yield approach zero. Soil water availability also decreases, falling below 1 mm in September, which limits ET to under 1 mm. This pattern reflects the water-limited conditions typical of semi-arid ecosystems, where ET is constrained primarily by soil moisture rather than atmospheric demand [61–65].

ET closely followed the seasonal precipitation cycle, peaking in March and April, coinciding with higher soil water content. Minimum values occurred between August and September, highlighting vegetation activity's dependence on rainfall. Such seasonal coupling of precipitation, soil moisture, and ET has also been reported in other semi-arid regions, where vegetation productivity and water fluxes respond rapidly to rainfall pulses [64–66].

Overall, sediment mobilization in the basin is strongly linked to the rainy season, while the system remains practically inactive during prolonged dry periods. This underscores rainfall seasonality as the primary driver of hydrological and erosive processes in semi-arid watersheds [65,66].

4.4. Spatial Variability and Controls of Hydrosedimentological Dynamics

The spatial distribution of variables such as soil water, surface runoff, SY, and ET is not uniform, being controlled by complex interactions between soil properties and LULC patterns. The spatial variability of these processes reveals distinct hydrological zones within the basin, which can be categorized from areas of high SY to regions of moisture accumulation.

ET varies between 184 and 855 mm in the basin, with the highest values in the northern areas of the basin, where the headwaters are located and near the outlet. ET values varied only slightly among soil classes, remaining relatively homogeneous overall. This homogeneous ET pattern can be attributed to semi-arid conditions, where soil water availability and precipitation variability exert a stronger influence on ET than the physical properties of soils. However, Luvisols showed a strong correlation with soil water availability, exhibiting a higher average ET and lower variability compared with the other soils.

The distribution of SY was predominantly influenced by the combination of bare soil and the Regosols soil type, which exhibited the higher average of SY. Regosols are shallow soils, generally less than 50 cm deep, typically occurring on gently undulating to mountainous terrain [67]. These soils have a coarse, predominantly sandy texture, which limits the maintenance of organic carbon, root stabilization, and water retention [68,69].

However, the high SY in these areas is not solely due to soil properties but is also linked to management practices. The widespread use of Regosols for livestock farming without conservation measures promotes soil compaction. This anthropogenic compaction reduces infiltration capacity, directly increasing surface runoff velocity and its power to detach and transport soil particles.

Both Leptosols and Regosols have pedogenetic similarities; however, in the study area, Regosols obtained a much higher SY volume. This is explained by the type of land use and position in the landscape. As Leptosols are associated with steeper slopes in this basin, this makes them unsuitable for agricultural practices, while Regosols are concentrated in flatter areas of the basin, which favors deforestation for non-conservationist livestock and goat farming in the region. Zewde et al. [70] when evaluated the SY in the Jemma Subbasin using the SWAT model also found higher SY estimated in Leptosols regions, and highlighted this is one of highly erodible soils exist in nature.

Even with these differences, both Regosols and Leptosols showed the lowest soil moisture content, consistent with their physical characteristics [70]. On the other hand, Luvisols, mainly situated in the lower basin near the watershed outlet, exhibited the

highest soil water levels, followed by Fluvisols, which displayed moderate water retention, reflecting their association with drainage channels [71]. These findings show the influence elevation on soil water content, where lower areas present higher soil water content than higher elevation areas.

Although Luvisols areas exhibit greater soil water storage in the soil, they also show greater sediment production. Similar results were found by Ayele et al. [72] when evaluating the spatial variability of sediment production in a watershed in Ethiopia, observed that Luvisols areas were also a floodplain prone to erosion and that extensive agriculture in a single dominant soil type (Luvisols) causes significant modifications in the landscape and sediment production.

Surface runoff was heterogeneous among soil classes, with Fluvisols exhibiting the greatest variability among soil types and experiencing the highest runoff. This is likely influenced by proximity to natural drainage networks and the geomorphology of the watershed, which demonstrates the contribution of surface runoff throughout the basin.

Even though Leptosols occur at higher elevations, they showed the lowest runoff because native vegetation cover is preserved. In contrast, Regosols exhibited higher runoff than Leptosols due to widespread deforestation of native vegetation, leading to high values of runoff and SY.

In general, native vegetation areas play a critical role in attenuating surface runoff during the rainy season due to their low runoff coefficients and high rates of evapotranspiration and soil water retention. In the Cachoeirinha basin, the greatest soil losses occur in areas of bare soil, whereas native vegetation exhibits a higher retention capacity.

Therefore, the presence of vegetation is fundamental in controlling SY. According to Bendito et al. [73], this result indicates that permanent soil cover, reduced erosivity, and conservation practices significantly contribute to minimizing both on-site and off-site soil loss impacts. Specifically, practices that increase surface roughness and infiltration are essential to decouple the link between high surface runoff and high SY in the basin.

In this context, Oliveira et al. [74], when evaluating the effects of LULC change on soil erosion in the dry forest "Caatinga", highlighted that areas of native vegetation (such as shrub caatinga) have been losing their natural cover, which has intensified soil loss. This dynamic pattern reinforces the interconnection between soil loss, LULC, and changes in vegetation cover over time.

4.5. Sediment Yield

The results demonstrated that the SY values are considered as low or mean range compared to other SY studies in similar regions. Temporally, the results showed a recent increase in SY between 2018 and 2023, compared to the previous window from 2013 to 2017, which was a period of historic drought. These results demonstrate that even in an environment with low precipitation, periods of higher rainfall intensity and SY can occur periodically, causing more erosion, especially in regions affected by poor soil management.

In this context, Silva et al. [75] using the SWAT model, observed substantially higher values, ranging from 128 t ha^{-1} yr^{-1} under natural conditions to 249 t ha^{-1} yr^{-1} on bare soil, emphasizing the critical role of LULC in regulating SY. In our study, bare soil was also a precursor to the largest areas of erosion, requiring caution in management systems to ensure soil cover. Similarly, Silva and Schulz [76] reported very high SY, with mean values around 138,619 t ha^{-1} yr^{-1}; however, climate and seasonality in the semi-arid environment limited sediment mobilization, with SY and monthly water distribution reaching R^2 = 0.88.

Soil erosion and sedimentation are critical global issues. Integrating conservation measures improves soil properties and reduces runoff. Understanding these impacts

enables farmers and managers to select effective, feasible erosion solutions for watersheds, both on- and off-site.

With this information, Silva et al. [77] evaluated different best management practices to reduce soil erosion and change water balance components in watersheds under grain and dairy production and found that the most effective in reducing soil erosion was crop rotation and cover crop (SY reduction of up to 38.4%). The authors found that the association of all conservation approaches was the most effective in reducing soil erosion followed by the vegetative measure scenario and that all combined scenarios increased infiltration and subsurface water components, and decreased surface runoff.

Conversely, the SY observed in this study aligns with reports of moderate to low rates. Piscoya et al. [78] recorded SY ranging from 0.45 to 1.72 t ha^{-1} yr^{-1}, closely matching the present average. Rabelo et al. [79] evaluated nine basins in the Brazilian semi-arid region and found SY values between 0.09 and 7.00 t ha^{-1} yr^{-1}, generally low due to limited precipitation and surface runoff, comparable to the maximum observed in this study. Bendito et al. [73] reported SY between 1.2 and 52.2 t ha^{-1} yr^{-1}, depending on the area, indicating that erosion is strongly influenced by anthropic activities and local erosivity.

These changes in land use, combined with the natural susceptibility of dry forest vegetation and soils in the region, make this environment unfavorable, decreasing the natural fertility of these soils and reducing biodiversity. Rainfall simulator experiments also illustrate the influence of LULC. Silva et al. [80] reported SY values under vegetative cover ranging from 0.053 t ha^{-1} for caatinga to 0.847 t ha^{-1} on maize, highlighting the role of land cover and experimental context. Similarly, Santos et al. [4], using the SWAT model, reported SY of 18.21 and 7.67 t ha^{-1} yr^{-1}, higher than the average in this study but still below extreme values reported elsewhere, confirming that surface runoff is a primary factor controlling SY highlighting the role of land use in amplifying or mitigating the effects of erosion.

These comparisons indicate that SY in the Brazilian semi-arid region, as observed in this study, aligns with reports of low sediment yield [78,79] and differs markedly from high-intensity SY scenarios at larger scales [75,76]. According to Viana et al. [81], SY is one of the variables most sensitive to changes in semi-arid environments than in humid environments, but generally, an increase in SY is associated with a combination of slope, soil erodibility, and the absence of conservation practices. These discrepancies are likely due to differences in study scale, local environmental conditions, LULC, and methodological approaches (field observation, simulation, or modeling).

A key result was that the highest sediment peak did not occur in the rainiest month (March), but in the transition month (January). This is because natural vegetation still has low leaf cover in January following the prior drought, leaving soil exposed to erosion from early rainfall. Since soils are predominantly shallow and poorly drained, runoff from these initial rains carried high sediment potential, which decreased slightly as seasonal vegetation cover increased.

4.6. Limitations and Model Applicability in Data-Scarce Regions

While the methodology applied in this study yielded satisfactory results, it is important to acknowledge certain limitations, particularly regarding the spatial resolution of satellite products. For ungauged basins, satellite-based ET estimates are still constrained by the lack of high-resolution products.

However, in data-scarce regions like the one analyzed here, the use of alternative variables for calibration, such as ET, becomes extremely relevant due to the paucity of flow monitoring stations. Andrade et al. [82] highlight that the absence of long-term (high-rate)

hydrometeorological data in semi-arid ungauged basins, and the lack of consistent data, make it challenging to model these regions. The semi-arid environment creates difficulties for hydrological models such as SWAT because these types of hydrological models struggle to produce results under semi-arid conditions, when soil are dry long periods of time.

Andrade et al. [82] noted that calibrating the SWAT model is generally easier during wet periods, when peak flows are more frequent than during dry periods, when flow generation is reduced. Given these constraints, prioritizing ET for calibration is scientifically justified. In semi-arid environments, ET accounts for a major portion of the water balance and is the primary pathway for water loss.

As highlighted by Lins et al. [50], ET is a critical component of the hydrological cycle in semi-arid regions, where high temperatures and significant crop water demand lead to elevated ET rates. Consequently, accurately representing ET is essential for effective water resource planning and management. Therefore, even in regions lacking high-resolution hydro-meteorological data, the SWAT model offers a valuable tool for approximating key hydrological processes at regional or broader scales.

5. Conclusions

SWAT behaved atypically compared to most studies in similar Brazilian environments, underestimating ET peaks during wet periods. During dry periods, however, ESTIMET observed ET showed better statistical results. High Nash–Sutcliffe Efficiency (NSE) and R^2 values were achieved, confirming the high potential of remote sensing for this calibration type. However, the moderate PBIAS values reflect the model's limitation in fully capturing ET peaks.

Regarding soil types, Regosols showed greater vulnerability to sediment yield. This is explained by their low capacity for plant development, coarse texture, and landscape position favorable to particle transport. In contrast, Leptosols, despite steeper slopes, exhibited less soil loss due to preserved native vegetation, as they are unsuitable for agriculture and maintain reasonable cover.

Surface runoff was the main driver of SY. The most affected areas were bare soil and Regosols. Therefore, the most effective mitigation strategy would be to adopt conservation practices that minimize surface water flow and maximize soil cover. In contrast, natural dry forest vegetation showed a lower capacity for SY retention compared to other land-use classes. This critical finding highlights the high sensitivity of this vegetation type to degradation and increasing aridity in Brazil's semi-arid regions.

Simulated SY values were relatively low and fell within ranges reported in other studies, indicating the model reliably represents SY under semi-arid conditions. Although rainfall events were intense, they were generally too brief to exceed soil infiltration capacity and generate substantial runoff. However, bare soil areas consistently produced the highest SY. SY tends to increase with medium to long term deforestation and reduced precipitation, which further exposes the soil.

The main limitations concerned model calibration. The manual process was time-consuming and required extensive parameter testing to achieve acceptable performance. Limited observed data availability restricted the evaluation of different hydrological components, increasing result uncertainty. Future studies should use automated calibration tools, incorporate additional observed data, and conduct sediment monitoring campaigns. Integrating multiple calibration targets, such as streamflow and sediment data, can further improve the model's predictive capacity and reliability under data-scarce conditions.

In the absence of standard observed data, ESTIMET evapotranspiration proved to be a reliable proxy for SWAT calibration. High statistical results were achieved using a free system, without the need for extensive fieldwork or a large team. It is important to note

that satellite calibration does not replace fieldwork and traditional monitoring but rather supports research where distance and accessibility to the study area are limiting factors.

Author Contributions: Conceptualization, R.G.d.S., A.M.S.d.C. and C.W.L.d.A.F.; methodology, R.G.d.S., A.M.S.d.C., C.M.d.A.C., V.H.R.C., A.A.d.A.M., C.W.L.d.A.F. and T.A.B.A.; software, R.G.d.S. and A.M.S.d.C.; validation, R.G.d.S. and A.A.d.A.M.; formal analysis, R.G.d.S.; investigation, R.G.d.S.; data curation, R.G.d.S., V.H.R.C. and C.M.d.A.C.; writing—original draft preparation, R.G.d.S., A.M.S.d.C., V.H.R.C. and M.A.d.S.; writing—review and editing, R.G.d.S., Y.J.A.B.d.S., V.H.R.C., A.M.S.d.C., C.W.L.d.A.F. and T.A.B.A.; supervision, R.G.d.S. and Y.J.A.B.d.S.; project administration, R.G.d.S. All authors have read and agreed to the published version of the manuscript.

Funding: The National Council for Scientific and Technological Development—CNPq (151969/2020-5, and 311.588/2023-9); The Brazilian Funding Authority for Studies and Projects—FINEP; the Foundation of Science and Technology Support for Pernambuco State—FACEPE (BFP-0092-5.03/24).

Institutional Review Board Statement: Not applicable.

Informed Consent Statement: Not applicable.

Data Availability Statement: The original contributions presented in this study are included in the article. Further inquiries can be directed to the corresponding author.

Conflicts of Interest: The authors declare no conflicts of interest.

References

1. United Nations Environment Programme. Report of the United Nations Conference on Desertification. In Proceedings of the United Nations Conference on Desertification, Nairobi, Kenya, 29 August–9 September 1977; United Nations Environment Programme: Nairobi, Kenya, 1977; p. 140.
2. Sterk, G.; Stoorvogel, J.J. Desertification—Scientific versus political realities. *Land* **2020**, *9*, 156. [CrossRef]
3. Teshome, D.S.; Leta, M.K.; Taddese, H.; Moshe, A.; Tolessa, T.; Ayele, G.; You, S. Watershed hydrological responses to land cover changes at Muger watershed, Upper Blue Nile river basin, Ethiopia. *Water* **2023**, *15*, 2533. [CrossRef]
4. Silva, I.A. Núcleos de desertificação do nordeste brasileiro: Suscetibilidade e dinâmica pluviométrica. *Os Desafios Geogr. Fís. Na Front. Conhecimento* **2017**, *1*, 1768–1776. [CrossRef]
5. Santos, J.; Andrade, E.; Medeiros, P.; Palácio, H.; Neto, J. Sediment delivery ratio in a small semi-arid watershed under conditions of low connectivity. *Rev. Ciênc. Agron.* **2017**, *48*, 49–58. [CrossRef]
6. Lane, L.J.; Hernandez, M.; Nichols, M. Processes controlling sediment yield from watersheds as functions of spatial scale. *Environ. Model. Softw.* **1997**, *12*, 355–369. [CrossRef]
7. White, K.L.; Chaubey, I. Sensitivity analysis, calibration, and validations for a multisite and multivariable SWAT model. *J. Am. Water Resour. Assoc.* **2005**, *41*, 1077–1089. [CrossRef]
8. Dutta, S. Soil erosion, sediment yield and sedimentation of reservoir: A review. *Model. Earth Syst. Environ.* **2016**, *2*, 123. [CrossRef]
9. Arnold, J.; Srinivasan, R.; Muttiah, R.S.; Williams, J.R. Large area hydrologic modeling and assessment Part I: Model development. *J. Am. Water Resour. Assoc.* **1998**, *34*, 73–89. [CrossRef]
10. Koutalakis, P.; Zaimes, G.; Ioannou, K.; Iakovglou, V. Application of the SWAT model on torrents of the Menoikio, Greece. *Fresen. Environ. Bull.* **2017**, *26*, 1210–1215.
11. Tufekcioglu, M.; Yavuz, M.; Zaimes, G.N.; Dinc, M.; Koutalakis, P.; Tufekcioglu, A. Application of Soil Water Assessment Tool (SWAT) to suppress wildfire at Bayam forest, Turkey. *J. Environ. Bio.* **2017**, *38*, 719. [CrossRef]
12. Souza, R.; Santos, I.; Kobiyama, M. O modelo SWAT como ferramenta para a gestão de recursos hídricos: Avaliação de vazões de outorga na bacia hidrográfica do Altíssimo Rio Negro. In Proceedings of the XVIII Simpósio Brasileiro de Recursos Hídricos, Campo Grande, Brazil, 22–26 November 2009.
13. Dantas, J.; Silva, M.; Silva, R.; Vianna, P. Simulação Vazão–Erosão usando o modelo SWAT para uma grande bacia da região semiárida da Paraíba. *Geociências* **2015**, *34*, 816–827.
14. Gassman, P.W.; Reyes, M.R.; Green, C.H.; Arnold, J.G. The Soil and Water Assessment Tool: Historical development, applications and future research directions. *Trans. ASABE* **2007**, *50*, 1211–1250. [CrossRef]
15. De Jesus Sales, J.; Netto, A.; Carvalho, C. Hydrological modeling of hydrographic basin in the northeast semi-arid region of Brazil. *Res. Soc. Develop.* **2022**, *11*, e48711326735. [CrossRef]

16. Echogdali, F.Z.; Boutaleb, S.; Taia, S.; Ouchchen, M.; Id-Belqas, M.; Kpan, R.B.; Abioui, M.; Aswathi, J.; Sajinkumar, K.S. Assessment of soil erosion risk in a semi-arid climate watershed using SWAT model: Case of Tata basin, South-East of Morocco. *Appl. Water Sci.* **2022**, *12*, 137. [CrossRef]
17. Mebarki, H.; Maref, N.; Dris, M. Modelling the monthly hydrological balance using Soil and Water Assessment Tool (SWAT) model: A case study of the Wadi Mina upstream watershed. *J. Groundwater. Sci. Eng.* **2024**, *12*, 161–177. [CrossRef]
18. Aragão, R.; Cruz, M.A.S.; Amorim, J.R.A.; Mendonça, L.C.; Figueiredo, E.E.; Srinivasan, V.S. Análise de sensibilidade dos parâmetros do modelo SWAT e simulação dos processos hidrossedimentológicos em uma bacia no agreste nordestino. *Rev. Bras. Ciênc. Solo* **2013**, *37*, 1091–1102. [CrossRef]
19. Collischonn, W.; Dornelles, M.F.; Castro, A.C.; Matsumoto, C.E. The MGB-IPH model for large-scale rainfall–runoff modelling. *Hydrol. Sci. J.* **2007**, *52*, 878–895. [CrossRef]
20. Avci, B.C.; Kesgin, E.; Atam, M.; Tan, R.I. Spatial-temporal response of sediment loads to climate change and soil conservation practices in the Northern Aegean Watershed, Türkiye. *Water* **2023**, *15*, 2461. [CrossRef]
21. Ware, H.H.; Chang, S.W.; Lee, J.E.; Chung, I.-M. Assessment of hydrological responses to land use and land cover changes in forest-dominated watershed using SWAT model. *Water* **2024**, *16*, 528. [CrossRef]
22. Passos, F.; Silva, B.C.; Silva, F.G.B. Avaliação de impactos de mudanças no uso e manejo do solo sobre as vazões da Bacia Hidrográfica do Ribeirão José Pereira, utilizando o modelo SWAT. *Rev. Bras. Geogr. Fís.* **2021**, *14*, 619–633. [CrossRef]
23. Kim, H.W.; Hwang, K.; Mu, Q.; Lee, S.O.; Choi, M. Validation of MODIS 16 global terrestrial evapotranspiration products in various climates and land cover types in Asia. *KSCE J. Civ. Eng.* **2012**, *16*, 229–238. [CrossRef]
24. Faisol, A.; Indarto, I.; Novita, E.; Budiyono, B. An evaluation of MODIS global evapotranspiration product as satellite-based evapotranspiration data for supporting precision agriculture in West Papua, Indonesia. *J. Tanah Trop.* **2021**, *26*, 43–49. [CrossRef]
25. Ruggieri, G.; Allocca, V.; Borfecchia, F.; Cusano, D.; Marsiglia, P.; De Vita, P. Testing Evapotranspiration Estimates Based on MODIS Satellite Data in the Assessment of the Groundwater Recharge of Karst Aquifers in Southern Italy. *Water* **2021**, *13*, 118. [CrossRef]
26. Maeda, E.; Ma, X.; Wagner, F.H.; Kim, H.; Oki, T.; Eamus, D.; Huete, A. Evapotranspiration seasonality across the Amazon Basin. *Earth Syst. Dynam.* **2017**, *8*, 439–454. [CrossRef]
27. Parajuli, P.; Jayakody, P.; Ouyang, Y. Evaluation of Using Remote Sensing Evapotranspiration Data in SWAT. *Water Resour. Manag.* **2018**, *32*, 985–996. [CrossRef]
28. Koltsida, E.; Kallioras, A. Multi-variable SWAT model calibration using satellite-based evapotranspiration data and streamflow. *Hydrology* **2022**, *9*, 112. [CrossRef]
29. Claudino, C.M.A.; Bertrand, G.F.; Nóbrega, R.L.B.; Almeida, C.N.; Gusmão, A.C.V.; Montenegro, S.M.G.L.; Silva, B.B.; Patriota, E.G.; Lemos, F.C.; Coutinho, J.V.; et al. ESTIMET: Enhanced and spatial-temporal improvement of MODIS evapotranspiration algorithm for all-sky conditions in tropical biomes. *Remote Sens. Environ.* **2025**, *325*, 114771. [CrossRef]
30. Soares, N.S.; Figueiredo, J.V.; Costa, C.A.G.; Rodrigues, I.S.; Araújo, J.C. Forest transpiration in Brazilian drylands: Measurement and validation of a hydrological model. *J. S. Am. Earth Sci.* **2025**, *170*, 105896. [CrossRef]
31. Medeiros, R.; Holanda, R.M.; Viana, M.A.; Silva, V.P. Climate classification in Köppen model for the state of Pernambuco–Brazil. *Rev. Geogr.* **2018**, *35*, 219–234. [CrossRef]
32. APAC. Agência Pernambucana de Águas e Clima. Registro de Pluviosidade em Pernambuco. 2023. Available online: http://www.apac.pe.gov.br (accessed on 22 August 2025).
33. Soares, W.A.; Silva, S.R.; Lima, J.R.S. Land-use change effect on the hydro-dynamic characteristics of soil in the Brazilian semi-arid region. *Rev. Ambiente Água* **2020**, *15*, e2368. [CrossRef]
34. Siva, C.V.T.; Andrade, E.M.; Filho, L.C.A.L.; Filho, J.C.R.; Júnior, H.S.O. Temporal dynamics of soil susceptibility to erosion in semiarid watersheds. *Acta Sci. Agron.* **2021**, *43*, e51378. [CrossRef]
35. Douglas-Mankin, K.R.; Srinivasan, R.; Arnold, J.G. Soil and Water Assessment Tool (SWAT) model: Current developments and applications. *Trans. ASABE* **2010**, *53*, 1423–1431. [CrossRef]
36. Williams, J.R.; Berndt, H.D. Sediment yield prediction based on watershed hydrology. *Trans. ASAE* **1977**, *20*, 1100–1104. [CrossRef]
37. Wischmeier, W.H.; Smith, D.D. *Predicting Rainfall Erosion Losses: A Guide to Conservation Planning*; United States Department of Agriculture, Science and Education Administration: Washington, DC, USA, 1978; p. 69.
38. Rallison, R.E.; Miller, N. Past, present and future SCS runoff procedure. In *Rainfall-Runoff Relationship: Proceedings of the International Symposium on Rainfall-Runoff Modeling*; Singh, V.P., Ed.; Water Resources Publications: Littleton, CO, USA, 1982; pp. 353–364. ISBN 0918334454.
39. MapBiomas. Coleção 8 da Série Anual de Mapas de Uso e Cobertura da Terra do Brasil. 2023. Available online: https://brasil.mapbiomas.org/ (accessed on 22 August 2025).
40. ZAPE. Zoneamento Agroecológico do Estado de Pernambuco. 2023. Available online: https://www.embrapa.br/busca-de-solucoes-tecnologicas/-/produto-servico/4697/zoneamento-agroecologico-do-estado-de-pernambuco-zape (accessed on 22 August 2025).

41. IBGE; Instituo Brasileiro de Geografia e Estatística. *Manual Técnico de Geomorfologia*, 2nd ed.; IBGE: Rio de Janeiro, Brazil, 2009; p. 182, ISBN 978-85-240-4110-5.
42. Monteith, J.L. Evaporation and environment in the state and movement of water in living organisms. *Symp. Soc. Exp. Biol.* **1965**, *13*, 205–234.
43. Arnold, J.G.; Moriasi, D.N.; Gassman, P.W.; Abbaspour, K.C.; White, M.J.; Srinivasan, R.; Santhi, C.; Harmel, R.D.; van Grienvesen, A.; van Liew, M.W.; et al. SWAT: Model use, calibration, and validation. *Trans. ASABE* **2012**, *55*, 1491–1508. [CrossRef]
44. Lins, F.A.C.; Montenegro, A.A.A.; Farias, C.W.L.A.; Chagas, A.M.S.; Miranda, R.Q.; Galvíncio, J.D. Análise da dinâmica temporal da evapotranspiração real em uma bacia hidrográfica do semiárido através de modelagem hidrológica e sensoriamento remoto. *Rev. IRRIGA Braz. J. Irrig. Drain.* **2021**, *26*, 543–564. [CrossRef]
45. Makumbura, R.K.; Gunathilake, M.B.; Samarasinghe, J.T.; Confesor, R.; Muttil, N.; Rathnayake, U. Comparison of Calibration Approaches of the Soil and Water Assessment Tool (SWAT) Model in a Tropical Watershed. *Hydrology* **2022**, *9*, 183. [CrossRef]
46. Collischonn, B.; Tucci, C. Relações regionais entre precipitação e evapotranspiração mensais. *Rev. Bras. Recur. Hídr.* **2014**, *19*, 205–214. [CrossRef]
47. Boyle, D.P.; Gupta, H.V.; Sorooshian, S. Toward improved calibration of hydrologic models: Combining the strengths of manual and automatic methods. *Water Resour. Res.* **2000**, *36*, 3663–3674. [CrossRef]
48. Gupta, H.V.; Sorooshian, S.; Yapo, P.O. Status of automatic calibration for hydrologic models: Comparison with multilevel expert calibration. *J. Hydrol. Eng.* **1999**, *4*, 135–143. [CrossRef]
49. Moriasi, D.N.; Arnold, J.G.; van Liew, M.W.; Bingner, R.L.; Veith, T.L. Model evaluation guidelines for systematic quantification of accuracy in watershed simulations. *Trans. ASABE* **2007**, *50*, 885–900. [CrossRef]
50. Lins, F.A.C.; Montenegro, A.A.A.; Farias, C.W.L.A.; Silva, M.V.; Souza, W.M.; Moura, G.B.A.; Silva, T.G.F.; Montenegro, S.M.G.L. Soil moisture and hydrological processes dynamics under climate and land use changes in a semiarid experimental basin, Brazil. *Ecohydrol. Hydrobiol.* **2024**, *24*, 681–697. [CrossRef]
51. Daramola, J.; Adepehin, E.J.; Ekhwan, T.M.; Choy, L.K.; Mokhtar, J.; Tabiti, T.S. Impacts of Land-Use Change, Associated Land-Use Area and Runoff on Watershed Sediment Yield: Implications from the Kaduna Watershed. *Water* **2022**, *14*, 325. [CrossRef]
52. Montenegro, A.; Ragab, R. Hydrological response of a Brazilian semi-arid catchment to different land use and climate change scenarios: A modelling study. *Hydrol. Process.* **2010**, *24*, 2705–2723. [CrossRef]
53. Silva, G.J.F.; Silva, R.M.; Neto, R.M.B.; Silva, J.F.C.B.C.; Dantas, A.P.X.; Santos, C.A.G. Multi-datasets to monitor and assess meteorological and hydrological droughts in a typical basin of the Brazilian semiarid region. *Environ. Monit. Assess.* **2024**, *196*, 368. [CrossRef] [PubMed]
54. Rocha, A.K.P.; Souza, L.S.B.; Montenegro, A.A.A.; Souza, W.M.; Silva, T.G.F. Revisiting the application of the SWAT model in arid and semi-arid regions: A selection from 2009 to 2022. *Theor. Appl. Climatol.* **2023**, *154*, 7. [CrossRef]
55. Zhang, L.; Xin, Z.; Zhang, C.; Song, C.; Zhou, H. Exploring the potential of satellite precipitation after bias correction in streamflow simulation in a semi-arid watershed in northeastern China. *J. Hydrol. Reg. Stud.* **2022**, *43*, 101192. [CrossRef]
56. Franco, A.C.L.; Bonumá, N.B. Multi-variable SWAT model calibration with remotely sensed evapotranspiration and observed flow. *RBRH-Rev. Bras. Recur. Hidricos* **2017**, *22*, 35. [CrossRef]
57. Magalhães, P.L.; Montenegro, A.A.A.; Andrade, C.W.L.; Montenegro, S.M.G.L.; Fontes Júnior, R.V.D.P. Hydrological modeling of an experimental basin in the semiarid region of the Brazilian State of Pernambuco. *Rev. Ambiente Água* **2018**, *13*, e2204. [CrossRef]
58. Fenta, A.A.; Yasuda, H.; Shimizu, K.; Haregeweyn, N.; Kawai, T.; Sultan, D.; Ebabu, K.; Belay, A.S. Spatial distribution and temporal trends of rainfall and erosivity in the Eastern Africa region. *Hydrol. Process.* **2017**, *31*, 4559–4573. [CrossRef]
59. García-Ruiz, J.M.; Beguería, S.; Nadal-Romero, E.; González-Hidalgo, J.C.; Lana-Renault, N.; Sanjuán, Y. A meta-analysis of soil erosion rates across the world. *Geomorphology* **2015**, *239*, 160–173. [CrossRef]
60. Costa, J.A.; Navarro-Hevia, J.; Costa, C.A.G.; Araújo, J.C. Temporal dynamics of evapotranspiration in semiarid native forests in Brazil and Spain using remote sensing. *Hydrol. Process.* **2021**, *35*, e14070. [CrossRef]
61. Oliveira, P.T.; Santos e Silva, C.M.; Lima, K.C. Climatology and trend analysis of extreme precipitation in subregions of Northeast Brazil. *Theor. Appl. Climatol.* **2017**, *130*, 77–90. [CrossRef]
62. Mu, Q.; Zhao, M.; Running, S.W. Improvements to a MODIS global terrestrial evapotranspiration algorithm. *Remote Sens. Environ.* **2011**, *115*, 1781–1800. [CrossRef]
63. Zhang, Y.; Peña-Arancibia, J.L.; McVicar, T.R.; Chiew, F.H.S.; Vaze, J.; Liu, C.; Lu, X.; Zheng, H.; Wang, Y.; Liu, Y.Y.; et al. Multi-decadal trends in global terrestrial evapotranspiration and its components. *Sci. Rep.* **2016**, *6*, 19124. [CrossRef]
64. Wilson, L. Seasonal sediment yield patterns of US rivers. *Water Resour. Res.* **1972**, *8*, 1470–1479. [CrossRef]
65. Jin, X.; Zhu, X.; Xue, Y. Satellite-based analysis of regional evapotranspiration trends in a semi-arid area. *Int. J. Remote Sens.* **2019**, *40*, 3267–3288. [CrossRef]
66. Yang, Z.; Zhang, Q.; Hao, X.; Yue, P. Changes in evapotranspiration over global semiarid regions 1984–2013. *J. Geophys. Res. Atmos.* **2019**, *124*, 2946–2963. [CrossRef]

67. Amogu, O.; Esteves, M.; Vandervaere, J.-P.; Abdou, M.M.; Panthou, G.; Rajot, J.-L.; Yéro, K.S.; Boubkraoui, S.; Lapetite, J.M.; Dessay, N.; et al. Runoff evolution due to land-use change in a small Sahelian catchment. *Hydrol. Sci. J.* **2015**, *60*, 78–95. [CrossRef]
68. Macedo, R.S.; Beirigo, R.M.; Medeiros, B.M.; Felix, V.J.L.; Souza, R.F.S.; Bakker, A.P. Processos pedogenéticos e susceptibilidade dos solos à degradação no semiárido brasileiro. *Rev. Caminhos Geogr.* **2021**, *22*, 176–195. [CrossRef]
69. Lima, J.R.S.; Oliveira, J.E.S.; Hammecker, C.; Duda, G.P.; Medeiros, E.V.; Antonino, A.C.D.; Souza, R.M.S.; Souza, E.S. Biochar increases soil water content and total organic carbon but has no effects on soil respiration in a Regosol of Caatinga. *Rev. Bras. Geogr. Fís.* **2020**, *13*, 3448–3458. [CrossRef]
70. Zewde, N.T.; Denboba, M.A.; Tadesse, S.A.; Getahun, Y.S. Predicting runoff and sediment yields using soil and water assessment tool (SWAT) model in the Jemma Subbasin of Upper Blue Nile, Central Ethiopia. *Environ. Chall.* **2024**, *14*, 100806. [CrossRef]
71. Pedron, F.; Fink, J.R.; Rodrigues, M.F.; Azevedo, A.C. Hydraulic conductivity and water retention in Leptosols–Regosols and saprolite derived from sandstone, Brazil. *Rev. Bras. Ciênc. Solo* **2011**, *35*, 1253–1262. [CrossRef]
72. Ayele, G.T.; Teshale, E.Z.; Yu, B.; Rutherfurd, I.D.; Jeong, J. Streamflow and sediment yield prediction for watershed prioritization in the Upper Blue Nile River Basin, Ethiopia. *Water* **2017**, *9*, 782. [CrossRef]
73. Bendito, B.P.C.; Chaves, H.M.L.; Scariot, A. Erosion and sedimentation processes in a semi-arid basin of the Brazilian Savanna under different land use, climate change, and conservation scenarios. *Water* **2023**, *15*, 563. [CrossRef]
74. Oliveira, N.M.; Silva, R.M.; Neto, R.M.B.; Santos, C.A.G.; Vianna, P.C.G. Spatiotemporal patterns of agricultural and meteorological droughts using SPI and MODIS-based estimates over a Brazilian semiarid region: Study case of Upper Paraíba River basin. *Geocarto Inter.* **2022**, *37*, 11590–11613. [CrossRef]
75. Silva, V.D.; Silva, M.T.; Souza, E.P. Influence of land use change on sediment yield: A case study of the sub-middle of the São Francisco river basin. *Eng. Agric.* **2016**, *36*, 1005–1015. [CrossRef]
76. Silva, T.P.; Bressiani, D.; Ebling, É.D.; Reichert, J.M. Best management practices to reduce soil erosion and change water balance components in watersheds under grain and dairy production. *Int. Soil Water Conserv. Res.* **2024**, *12*, 121–136. [CrossRef]
77. Silva, A.M.; Schulz, H.E. Hydrosedimentological dynamic on Água Fria watershed. *Braz. Arch. Biol. Technol.* **2007**, *50*, 861–870. [CrossRef]
78. Piscoya, V.C.; Melo, R.C.P.; Filho, M.C.; Guerra, S.M.S.; Piscoya, T.O.F.; Filho, R.R.G.; Fernandes, M.M.; Pedrotti, A.; Holanda, F.S.R.; Filho, R.N.A. Sediment delivery ratio from a small semiarid watershed of Brazil. *Rev. Bras. Geogr. Fís.* **2021**, *14*, 1586–1596. [CrossRef]
79. Rabelo, D.R.; Cavalcante, A.A.; Araújo, J.C. Sediment yield in a basin in Brazilian Semiarid Regions: A discussion on positive allometry. *CATENA* **2023**, *221*, 106749. [CrossRef]
80. Silva, R.M.; Santos, C.A.G.; Santos, J.Y.G. Evaluation and modeling of runoff and sediment yield for different land covers under simulated rain in a semiarid region of Brazil. *Int. J. Sediment Res.* **2018**, *33*, 117–125. [CrossRef]
81. Viana, J.F.S.; Montenegro, S.M.G.L.; Srinivasan, R.; Santos, C.A.G.; Mishra, M.; Kalumba, A.M.; Silva, R.M. Land Use and Land Cover Trends and Their Impact on Streamflow and Sediment Yield in a Humid Basin of Brazil's Atlantic Forest Biome. *Diversity* **2023**, *15*, 1220. [CrossRef]
82. Andrade, H.M.L.; Montenegro, A.A.A.; Andrade, C.W.L.; Montenegro, S.M.G.L.; Júnior, R.V.P.F. Soil moisture and discharge modeling in a representative watershed in northeastern Brazil using SWAT. *Water Resour. Manag.* **2019**, *33*, 123–137. [CrossRef]

Disclaimer/Publisher's Note: The statements, opinions and data contained in all publications are solely those of the individual author(s) and contributor(s) and not of MDPI and/or the editor(s). MDPI and/or the editor(s) disclaim responsibility for any injury to people or property resulting from any ideas, methods, instructions or products referred to in the content.